ISTANBUL TECHNICAL UNIVERSITY ★ GRADUATE SCHOOL OF SCIENCE ENGINEERING AND TECHNOLOGY

STRUCTURAL AND OPTICAL PROPERTIES OF MODIFIED TITANIUM DIOXIDE BASED FILMS PREPARED BY SOL-GEL DIP-COATING

M.Sc. THESIS

Houman BAHMANI JALALI

Department of Nano Science and Nano Engineering

Nano Science and Nano Engineering Programme

JUNE 2015

ISTANBUL TECHNICAL UNIVERSITY ★ GRADUATE SCHOOL OF SCIENCE ENGINEERING AND TECHNOLOGY

STRUCTURAL AND OPTICAL PROPERTIES OF MODIFIED TITANIUM DIOXIDE BASED FILMS PREPARED BY SOL-GEL DIP-COATING

M.Sc. THESIS

Houman BAHMANI JALALI
(513131013)

Department of Nano Science and Nano Engineering

Nano Science and Nano Engineering Programme

Thesis Advisor: Prof. Dr. Levent TRABZON

JUNE 2015

İSTANBUL TEKNİK ÜNİVERSİTESİ ★ FEN BİLİMLERİ ENSTİTÜSÜ

SOL-JEL DALDIRMA YÖNTEMİ İLE HAZIRLANAN MODİFİYE TİTANYUM DİOKSİT TABANLI FİLMLERİN YAPISAL VE OPTİK ÖZELLİKLERİ

YÜKSEK LİSANS TEZİ

Houman BAHMANİ JALALİ
(513131013)

Nano Bilimi ve Nano Mühendisliği Anabilim Dalı

Nano Bilimi ve Nano Mühendisliği Programı

Tez Danışmanı: Prof. Dr. Levent TRABZON

HAZİRAN 2015

Houman BAHMANI JALALI, a **M.Sc.** student of ITU **Graduate School of Science and Engineering** student ID 513131013, successfully defended the **thesis** entitled "**STRUCTURAL AND OPTICAL PROPERTIES OF MODIFIED TITANIUM DIOXIDE BASED FILMS PREPARED BY SOL-GEL DIP-COATING**", which he prepared after fulfilling the requirements specified in the associated legislations, before the jury whose signatures are below.

Thesis Advisor :	**Prof. Dr. Levent TRABZON** Istanbul Technical University	.....
Jury Members :	**Assoc. Prof. Dr. Hüseyin KIZIL** Istanbul Technical University	.....
	Assoc. Prof. Dr. Kaşif TEKER Istanbul Şehir University	.....

Date of Submission : 4 May 2015
Date of Defense : 8 June 2015

To my mother, Nadereh AHMADPOUR

FOREWORD

I would like to express my deepest gratitude to my supervisor, Prof. Dr. Levent Trabzon for giving me an opportunity to work in this project at ITUnano Nanotechnology Research Center, for his guidance, support and encouragement during the entire course of this work.

My sincere thanks to Associate Prof. Hüseyin Kızıl for the immense support and friendly cooperation.

Special thank to Dr. Esra Özkan Zayim and Dr. Hakan Karaağaç for the helpful guidence about optical characterization.

I would like to thank my deepest thank to Meisam Farzalipour Tabriz and Ahmad Esmaeilzadeh Kandjani for their effective and innovative guidence. I would also like to thank all my friends and all staff at the ITUnano Nanotechnology Research Center and ITU-MEMS for providing the supportive working environment, especially to my laboratory colleagues Mumin Balaban and Muhammed Bekin. The author thanks Hatice Turhan for her assistence and Kaveh Rahimzadeh Berenji for his help in the thesis template arrangement.

Finally, I would like to thank my father Mohammad Bahmani Jalali, for all his love and support.

June 2015 Houman BAHMANI JALALI

TABLE OF CONTENTS

Page

ABBREVIATIONS

Ag	**:** Silver
EDS	**:** Enery Disperse Spectroscopy
FT-IR	**:** Fourier Transform Infrared
Fe	**:** Iron
IR	**:** Infrared
N	**:** Nitrogen
SEM	**:** Scanning Electron Microscopy
TiO_2	**:** Titanium Dioxide
UV-Vis	**:** Ultra Violet –Visible
XRD	**:** X-ray Diffraction
XPS	**:** X-ray Photoelectron Spectroscopy
ZnO	**:** Zinc Oxide

LIST OF TABLES

Page

LIST OF FIGURES

Page

STRUCTURAL AND OPTICAL PROPERTIES OF MODIFIED TITANIUM DIOXIDE FILMS PREPARED BY SOL-GEL DIP-COATING

SUMMARY

In this study, several modified titanium dioxide films were prepared via sol-gel dip-coating method and their structural and optical properties were investigated. Several forms of modified TiO_2 films such as metal doped TiO_2, nonmetal doped TiO_2, metal-nonmetal co-doped TiO_2, silver decorated TiO_2 and composite TiO_2 were prepared and characterized.

Firstly, pure titanium dioxide sol was prepared following optimized sol recipe. Prepared sol was transparent, homogeneous and no precipitation was occurred. Pure TiO_2 thin film was prepared by sol-gel dip-coating method and its structural and optical characterizations were investigated. It was seen that the crystal structure of pure TiO_2 thin film was fully anatase. The XPS survey shows that position of the Ti 2p3/2 peak is close to the reported value by reference and the oxidation level of titanium is +4 as expected. The SEM image reveals that pure TiO_2 sample has a homogeneous structure with a particle size between 20 nm and 30nm. The optical absorption edge of the pure TiO_2 sample is around 350 nm. The band-gap value was calculated using UV transmission data by Tauc plot method. The band gap of pure TiO_2 is about 3.55 eV, which is higher than the reported band gap value for crystalline anatase TiO_2.

We have prepared nitrogen doped TiO_2 thin films via so-gel method as nonmetal doped TiO_2 and the effect of nitrogen doping and dopant concentration on structural and optical characterization of TiO_2 were studied. It was found that increasing the dopant concentration doesn’t decrease the band-gap value and have no effect on crystal structure. Sample doped with 1.5 wt% nitrogen has lowest band-gap value.

Iron doped TiO_2 thin films with different dopant concentration were prepared and the effect of iron doping and dopant concentration on structural and optical properties of TiO_2 were investigated. It was concluded that the band-gap value is decreasing by increasing the dopant concentration. The absorption edge of sample doped with 3 wt% iron relies on visible light region.

Silver doped TiO_2 thin films with different dopant concentration were prepared and the influence of silver doping and dopant concentration on structural and optical characterization of TiO_2 were investigated. The optical absorbance of Ag-doped TiO_2 thin films state that the wavelength of the absorption edge does not increase by increasing the dopant concentration. The absorption edge of silver doped samples rely on UV region.

We studied three different 3 wt% nitrogen-iron co-doped TiO_2 films with different dopants ratio and results are compared with pure TiO_2 film. The resulting sols were homogeneous and transparent and no precipitation was observed in any of them. It was seen that dopants ratio changes the opacity of prepared samples and sample with medium dopants concentration was opaque in a short time after dip-coating process. It was found that the dopants ratio has effect on the crystal structure, microstructure, surface morphology and optical properties of the resulting films. Sample with medium dopants concentration has amorphous structure and bigger particle size. We also found that crystalline structure, surface morphology and its optical properties are dependent on dopants ratio of N-Fe co-doped TiO_2 films.

Silver decorated TiO_2 films were prepared. Firstly pure TiO_2 thin films were prepared as mentioned above and were dip-coated in silver nitrate aqueous solution. The idea of the preparation of Silver decorated TiO_2 films was the photo-decomposition and thermal-decomposition of silver nitrate to metal silver. Several photo-decomposed and thermal-decomposed have been prepared and their optical and structural properties were studied and compared. The surface elemental analysis of photo-decomposed sample reveals the presence of titanium and oxygen element as expected and the silver amount is around 7 atomic percent. Although the surface elemental analysis of thermal decomposed sample shows the presence of titanium and oxygen element as expected but the amount of silver is too low in comparison with photo-decomposed sample. It can be concluded that the silver reduction of photo-decomposition is much higher than thermal-decomposition. The optical absorbance of silver decorated TiO_2 thin films states that the optical properties of TiO_2 is affected negatively by thermal decomposition of silver nitrate. The absorption edge of the photo-decomposed sample relies on visible light region.

Pure ZnO thin film was prepared and the results show that the band gap of pure ZnO is around 3.6 eV which is higher than reported 3.4 eV.

TiO_2 @ ZnO composite films have been prepared by sol-gel dip-coating method and the effect of sol molar ratio on optical properties of the films were investigated. Three different samples with different titanium to zinc molar ratios were prepared. The absorption edge of TiO_2 rich sample is close to the pure TiO_2 absorption edge and the absorption edge of ZnO rich sample is close to the pure ZnO absorption edge.

SOL-JEL DALDIRMA YÖNTEMİ İLE HAZIRLANAN MODİFİYE TİTANYUM DİOKSİT TABANLI FİLMLERİN YAPISAL VE OPTİK ÖZELLİKLERİ

ÖZET

Bu çalışmada sol-gel dip-coating yöntemi ile çeşitli modifiye titaniyum dioksit tabanlı filmler hazırlanmış ve yapısal ve optik özellikleri karakterize edilmiştir. Modifiye titanyum dioksit olarak metal katkılı, ametal katkılı, metal-ametal katkılı, gümüş dekoreli ve kompozit filmler sol-jel yöntemi ile hazırlanmıştır.

Moleküler ön başlatıcıların hidroliz ve kondenzasyonuna dayanan sol- jel sentezi, inorganik malzemeler hazırlamak için geniş bir yelpazede kullanılmaktadır. Sol- jel tekniği hem inorganik hem de organik-inorganik hibrit polimerlerin elde edilmesinde çok kullanışlı bir yöntemdir. Bu tekniğin temel avantajı tüm prosesin oldukça ılımlı koşullarda yürütülmesidir. Katı hal proseslerinin aksine sol- jel prosesi, son ürüne ön başlatıcı türlerinin dönüşümü sırasında reaksiyon yolunda moleküler seviyede kontrol imkânı sunmaktadır. Böylece sol- jel prosesi, çok yüksek saflık ve homojenlikte, uniform kristal morfolojisinde ve iyi tanımlanmış nanopartiküllerin sentezine olanak sağlar. Sol- jel kimyası, bir yandan suyun ligand oluşturma ve çözücü olarak çift rolü ve metal oksit ön başlatıcılarının suya karşı reaktivitesinden dolayı, ve diğer yandan sentez protokolünün iyi tekrarlanabilirliğini sağlamak için sıkı bir şekilde kontrol edilmesi gereken reaksiyon parametrelerinin çok sayısında olması (metal alkokst ön başlatıcılarının hidroliz ve kondenzasyon hızı, pH, sıcaklık, karıştırma yöntemi, oksidasyon hızı, vb.) nedeniyle oldukça karmaşık bir prosestir. Bu nedenle derlemenin ana hedefi sol-jel prosesinin temel prensibini anlatmak ve proseste etkili olan parametreleri irdelemektir.
Bu yöntem atmosferik durumlarda ve kontrol altındaki sıcaklıklarda bir alt tabakanın belirlenmis bir hızda hazırlanan çözeltinin içine daldırılıp geri çekilmesiyle kaplama yapılan bir yöntemdir. Daldırma sırasında alt tabakanın sarsıntısız ve

oldukça düzgün hareketi sağlanmalıdır. İnce ve düzgün kaplama akıcı bir yüzeye, alt tabakanın minimum titreşimine ve doğru hız kontrolüne bağlıdır. Kaplama kalınlığı esas olarak çekiş hızı, katının kalınlığı ve sıvının akışkanlığına bağlı olarak tanımlanır. Alkol gibi çözücülerle yapılan kaplamalarda, süzülme safhasına gerek yoktur. Hareket halindeki taşıyıcı, sole daldırıldığı an akışkanlar mekaniği gereği kaplama alanı üzerinde sol ihtiva eden bir sınır tabaka olusur. Kaplama ve süzülme aşamasında sözü edilen sınır tabaka, iç tabaka ve dış tabaka olmak üzere ikiye ayrılır. İç tabaka tasıyıcı ile birlikte hareket ederken dış tabaka ters yöne dogru hareket ederek sole geri döner. Filmin kalınlığı aşağı ve yukarı hareket eden tabakaları ayıran ana akıntının şiddetine bağlıdır.

Ametal katkılı titanyum dioksit olarak nitrojen katkılı TiO_2 filmleri sol-jel yöntemi ile hazırlanmış ve titanyum diyoksitin yapısal ve optik özellikleri üzerinde nitrojen katkısı ve katkı konsantrasyonunun etkisi incelenmiştir. Nitrojen katkı konsantrasyonu arttıkça band-gap değerinin düşmediği gözlenmiştir. Ayrıca nitrojen katkısının kristal yapıya etkisi olmadığı görülmüştür.

Metal katkılı titanyum dioksit olarak demir katkılı TiO_2 filmleri sol-jel yöntemi ile hazırlanmış ve titanyum dioksitin yapısal ve optik özellikleri üzerinde demir katkısı ve katkı konsantrasyonunun etkisi incelenmiştir. Demir katkı konsantrasyonu arttıkça band-gap değerinin düşdüğü gözlenmiştir. Ayrıca demir katkısı kristal yapıya etkisi olmadığı görülmüştür.

Metal katkılı titanyum dioksit olarak gümüş katkılı TiO_2 filmleri sol-jel yöntemi ile hazırlanmış ve titanyum dioksitin yapısal ve optik özellikleri üzerinde gümüş katkısı ve katkı konsantrasyonunun etkisi incelenmiştir. Gümüş katkı konsantrasyonu arttıkça band-gap değerinin düşmedüğü gözlenmiştir.

Metal ametal çift katkılı titanyum dioksit olarak nitrojen demir çift katkılı TiO_2 filmleri sol-jel yöntemi ile hazırlanmış ve titanyum dioksitin yapısal ve optik özellikleri üzerinde katkısı ve katkı konsantrasyonunun etkisi incelenmiştir. Katkı oranlarının titanyum dioksitin yapısal ve optik özelliklerine etkili olduğu görünmüştür.

Kompozit titanyum dioksit olarak TiO_2 @ ZnO kompozit filmleri sol-jel yöntemi ile hazırlanmış ve titanyum/çinko oranının optik özellikleri üzerindeki etkisi incelenmiştir.

1. INTRODUCTION

Titanium dioxide (TiO_2) is a material used in a wide range of common and high-tech applications. It is cheap, chemically stable, non-toxic, and last but not least biocompatible. Titanium is successfully used as implant material for dental, orthopedic and osteosynthesis application and its native oxide is mostly constituted of titanium dioxide. TiO_2 powder is used as white pigment in paint [1], replacing lead oxide which is toxic, and in toothpaste. Transparent single crystals or thin films have a high refractive index that makes TiO_2 suitable for optical applications [2-4]. Multi-layers composed of TiO_2 and SiO_2 are designed to make antireflection coatings in the whole visible range [5, 6]. TiO_2 is widely used for photocatalysis [7], for example for water treatment by oxidation of dissolved organic molecules. Electrodes made of TiO_2 are used in electrochromic devices and dye-sensitized solar cells [8]. Pd-TiO_2 diodes are used as hydrogen gas sensor [9, 10], it can replace ZrO_2 in lambda probes used in the car industry. Thus, research in many different fields is devoted to titanium dioxide under various forms such as single crystals, ceramics, and thin films.

2. TITANIUM DIOXIDE

This chapter gives information necessary to understand the structure and main characteristics of TiO_2 thin films. It starts with a description of the different polymorphs of titanium dioxide. Then, a short reminder the properties of semiconductors are presented.

2.1 General Properties of TiO_2

The titanium oxide can crystallize in different structures. At ambient conditions, four structures are known: rutile, anatase, brookite, and srilankite [11]. At higher pressure, i.e. more than 10 GPa, a baddeleyite structure appears [12], and theoretical work predicts a new structure, not yet observed, similar to fluorite HfO_2 at even higher pressure[13]. The most stable phase of TiO_2 is rutile crystal structure[14]. The brookite structure has been obtained by the sol-gel method[15, 16], and TiO_2-II (srilankite) has been grown by atomic layer epitaxy from $TiCl_4$ and H_2O [17]. General properties of anatase, rutile, brookite is reported in table below.

Table 2.1 : Ploymorphs of TiO_2.

Polymorph	Anatase	Rutile	Brookite
Structure	tetragonal $I4_1/amd$	tetragonal $P4_2/mnm$	orthorhombic P_{cab}
Density	3.89	4.25	4.37
Refractive index	2.55	2.6	2.57
Bang-gap (eV) [18]	3.42	3.04	3.14

The elementary cells of the TiO_2 crystal structures are presented in Figure 2.1. Rutile and anatase, which are tetragonal, are more ordered than the orthorhombic structure. The anatase, which is the least dense structure, has empty channels along the a and b axes.

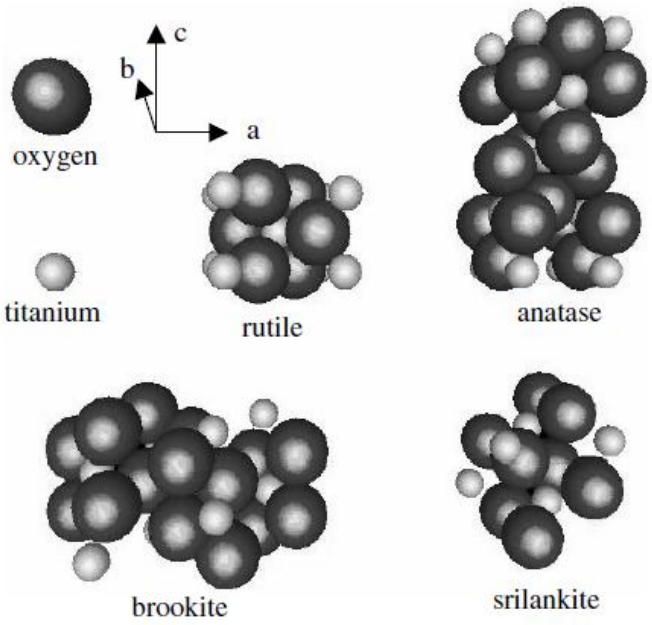

Figure 2.1 : Elementary cell of different polymorphs of TiO_2 [18].

When the titanium oxide stoichiometry is varied from 0 to 2, Ti, Ti_2O, TiO, Ti_2O_3, Ti_3O_5, Ti_nO_{2n-1}, and TiO_2 are encountered. Rutile and anatase structures are compatible with stoichiometries higher than 1.95 only. No titanium oxide structure with a stoichiometry higher than 2 has been reported.

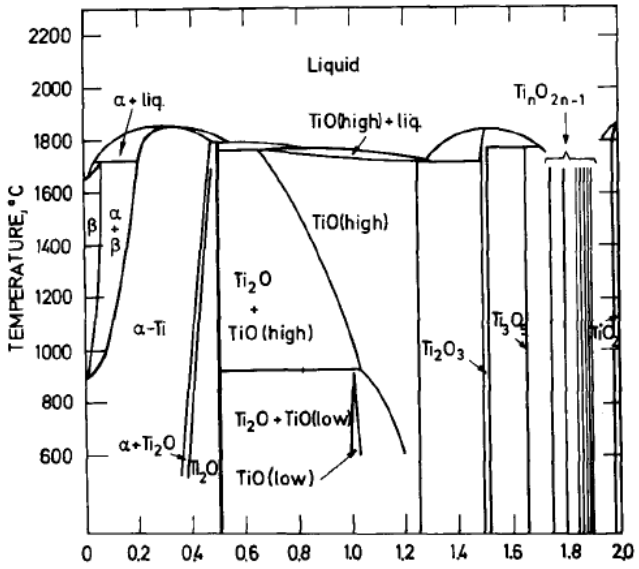

Figure 2.2 : The titanium oxygen phase diagram [19].

Rutile can exist at any temperature below 1800°C, at which point titanium dioxide becomes liquid, while for temperatures above 700°C the anatase structure changes to the rutile structure [20]. To our knowledge, the reverse transformation never occurs. The transformation temperature can be modified by adding impurities

into TiO_2. For instance, the anatase phase completely disappears at temperature of about 530°C, 680°C, and 830°C for powder samples containing vanadium, molybdenum, and tungsten respectively [21].

In the following, the description of the properties of titanium oxide will be focussed on the anatase polymorphs of TiO_2 because it is the only polymorphs synthesized in our thin films.

Among the different commercially available titanium dioxides, the commercial Degussa product P25 is one of the most frequently applied ones in photocatalysis because it shows high activity for many kinds of photocatalytic reactions, probably due to its exceptional structure. It has often been proposed for the degradation of pollutants in water or air. The product is manufactured by flame hydrolysis (Aerosil process). The specifications of the product P25 TiO_2 are listed in Table below.

Table 2.2 : Specifications of Degussa P-25.

Crystalline type	Crystalline size	BET specific surface area
Anatase(80%)+Rutile(20%)	25nm	50 m2g-1

2.2 Semiconductor

A semiconductor, by solid state definition, is a material whose valence band (VB) and conduction band (CB) are separated by an energy gap or band gap (Ebg). A conductor is distinguished by having a partially filled conduction band, the valence band overlaps the conduction band and there is no energy band gap. If the energy separation between the valence band and the conduction band is large (greater than 5 eV), the material is an electrical insulator.

Activation of a semiconductor photocatalyst is achieved by means of the adsorption of a photon energy (E_{ph}) which results in the promotion of an electron, e^- , from the valence band into the conduction band with the generation of a hole, h^+, in the valence band of the catalyst, according to Eq. 2.1 and the reaction illustrated in Figure 2.1

In metals, where there is a continuum of energy states, the light-generated electrons deactivate easily and the lifetime of the electron-hole pair is so short that they cannot

be harvested. The existence of a band gap in semiconductors prevents rapid deactivation of the excited electron-hole pairs, which can be deactivated only by recombination. This assures that an electron-hole pair lifetime is sufficiently long to participate in interfacial electron transfer[22]. In an oxygenated aqueous suspension, redox reactions are produced which can oxidize organic compounds[23].

Various chemical steps occur in the photocatalytic reactions, following the initiation step of pair electron-hole formation. This lead to the utilization of both the electron hole h^+ for the oxidation processes and eventually to the capture of the e^- electron for the reduction processes, as well the potential formation of super oxide anions and hydrogen peroxide from oxygen (de Lasa, Serrano et al. 2005).

Iron oxides are no suitable semiconductors, even though they are inexpensive and have high band gap energies, because they readily undergo photocathodic corrosion[24]. ZnO appears suitable for photocatalysis due to its band gap energy is (3.2 eV), however, ZnO is generally unstable in solution even without irradiation, especially at low pH [25]. Utilization of WO_3 as a photocatalyst has also been investigated; nevertheless it shows a lower photocatalytic activity than TiO_2[25, 26].

Among the other semiconductors TiO_2 is the most commonly applied catalyst due to several favorable factors: it is highly photoactive, very photostable, biologically and chemically inert, non-toxic and also inexpensive [23, 24].

2.3 Photocatalysis

The word photocatalysis is composed of two parts, “photo” and “catalysis”. Catalysis is the process where a substance participates in modifying the rate of a chemical transformation of the reactants without being altered or consumed in the end. This substance is known as the catalyst which increases the rate of a reaction by reducing the activation energy.

Photocatalysis is a reaction which uses light to activate a substance which modifies the rate of a chemical reaction without being involved itself. And the photocatalyst is the substance which can modify the rate of chemical reaction using light irradiation.

Chlorophyll of plants is a typical natural photocatalyst. The difference between chlorophyll photocatalyst to synthetic nano TiO_2 photocatalyst (here below mentioned as photocatalyst) is, usually chlorophyll captures sunlight to turn water and carbon dioxide into oxygen and glucose, but on the contrary photocatalyst creates strong oxidation agent and electronic holes to breakdown the organic matter to carbon dioxide and water in the presence of photocatalyst, light and water.

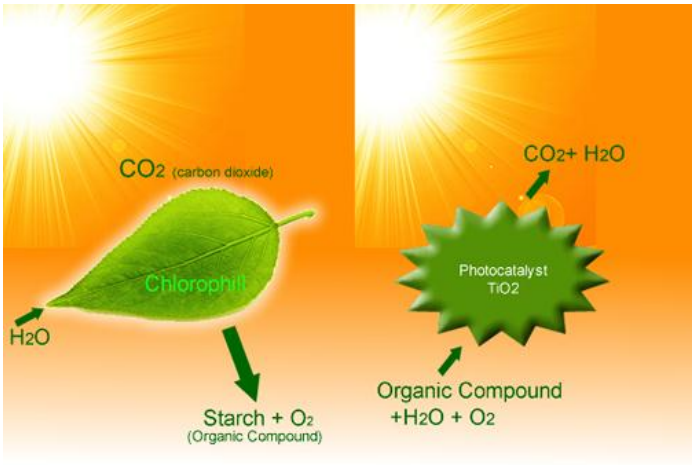

Figure 2.3 : Natural and synthetic photocalalysts.

2.3.1 Hystorical overview of TiO_2 photocatalysis

The important breakthroughs in the research on TiO_2 photocatalysis that have led to many practical applications are summarized below.

In 1972, K. Honda and A. Fujishima discovered the photosensitization effect of a TiO2 electrode for the electrolysis of H_2O into H_2 and O_2 using a Pt metal electrode as cathode and a TiO_2 photoanode irradiated with UV light. They found that, under UV light irradiation of the TiO_2 electrode, the electrolysis of H_2O proceeded at a much lower bias voltage as compared to normal electrolysis [27].

2.3.2 General mechanism of photocatalysis

When photocatalyst titanium dioxide absorbs Ultraviolet radiation from sunlight or illuminated light source (fluorescent lamps), it will produce pairs of electrons and holes. The electron of the valence band of titanium dioxide becomes excited when illuminated by light. The excess energy of this excited electron promoted the electron to the conduction band of titanium dioxide therefore creating the negative-electron

(e-) and positive-hole (h+) pair. This stage is referred as the semiconductor's 'photo-excitation' state. The energy difference between the valence band and the conduction band is known as the 'Band Gap'. Wavelength of the light necessary for photo-excitation is: 1240 (Planck's constant, h) / 3.2 ev (band gap energy) = 388 nm

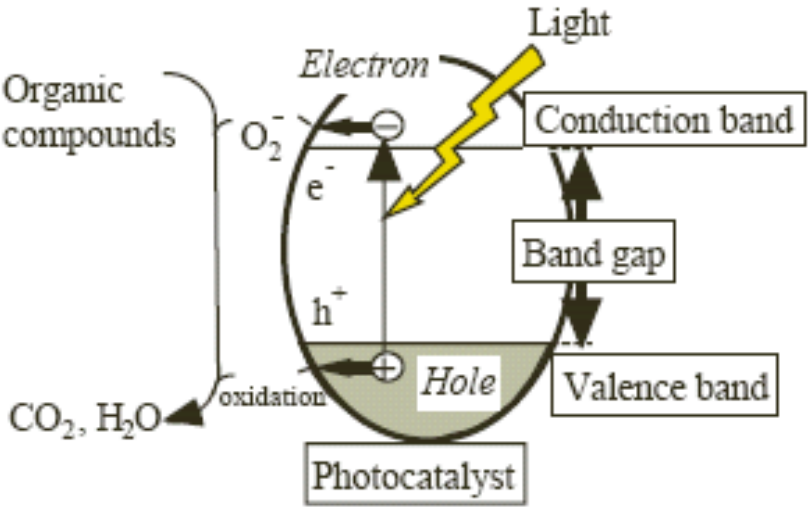

Figure 2.4 : General mechanism of photocatalysis.

The positive-hole of titanium dioxide breaks apart the water molecule to form hydrogen gas and hydroxyl radical. The negative-electron reacts with oxygen molecule to form super oxide anion. This cycle continues when light is available.

2.3.3 Primary steps in mechanism of photocatalysis

However, the detailed mechanism of photocatalysis varies with different pollutants, it is commonly agreed that the primary reactions responsible for the photocatalytic effect are interfacial redox reactions of electrons and holes that are generated when the semiconductor catalyst is exposed to light of sufficient energy [28-30]. Primary steps in the mechanism of photocatalysis are summarized below and shown in Fig below

(1) Formation of charge carriers by photon absorption

(2) Charge carrier recombination

(3) Trapping of a conduction-band electron at a Ti(IV) site to yield Ti(III)

(4) Trapping of a valence-band hole at a surficial titanol group

(5) Initiation of an oxidative pathway by a valence-band hole

(6) Initiation of a reductive pathway by a conduction-band electron

(7) Further thermal (e.g., hydrolysis or reactions with active oxygen species) and photocatalytic reactions to yield mineralization products.

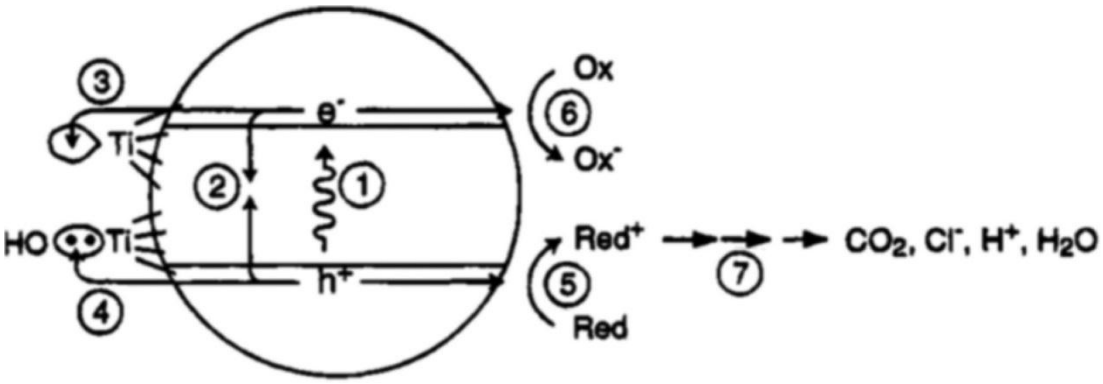

Figure 2.5 : Primary steps in the mechanism of photocatalysis [24].

The reaction dynamics of the photogenerated charge carriers in TiO2, shown in Figure 5, are usually obtained by means of time-resolved absorption spectroscopy (TAS), being a widely employed technique to study the formation, relaxation, recombination, and transfer processes of photogenerated charge carriers in photocatalysts. While during the past decade, the measuring techniques have been improved, and it is, e.g., now possible to measure on the femtosecond time scale, a meaningful interpretation of the observed kinetics or even a chemical assignment of the detected absorption transients has rarely been executed.

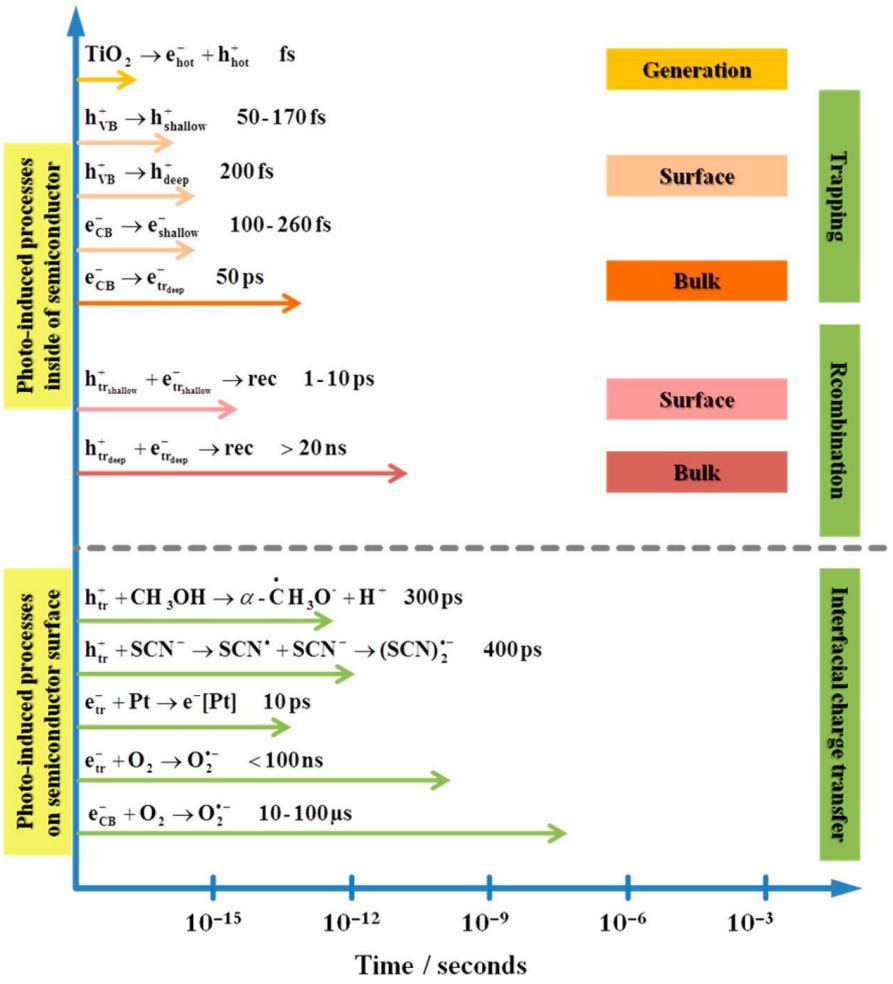

Figure 2.6 : Photoinduced reactions in photoatalysis of TiO_2 and the corresponding time scales.

2.3.4 Present applications of photocatalysts

The commercialization of TiO_2 based photocatalytic products commenced in the mid-1990s in Japan. However, this industry has grown very quickly, and its market reached ca. 30 billion Japanese yen in Japan in 2003. More than 2000 companies have joined in this new industry, whose products can be mainly divided into five categories, i.e. exterior construction materials, interior furnishing materials, road construction materials, purification facilities, and household goods, etc., as shown in Table 1.

TiO2-based self-cleaning exterior products, includ- ing tiles, glass, tents, etc., have been widely applied in Japan. Such products can keep clean by the action of sunlight and rainwater, based on the photocatalytic and superhydrophilic properties of TiO2. That is, as shown in Fig. 7, gradually adsorbed organic soilage such as oil is decomposed by the photocatalytic property of TiO2, while organic contaminants and

dust can be washed off by rainwater because of the superhydro- philic property of TiO2. It is not true that a superhydro- philic self-cleaning surface will never turn dirty, since the self-cleaning process is dependent on the illumina- tion conditions of sunlight, the amount of rainfall, and the accumulation rate of soilage, etc. But it is really true that such a self-cleaning surface will retard the rate of contamination, and thus save a lot of time and cost for cleaning maintenance, which is very difficult for high buildings and flexible plastic materials (e.g. domes, canopies and tents).

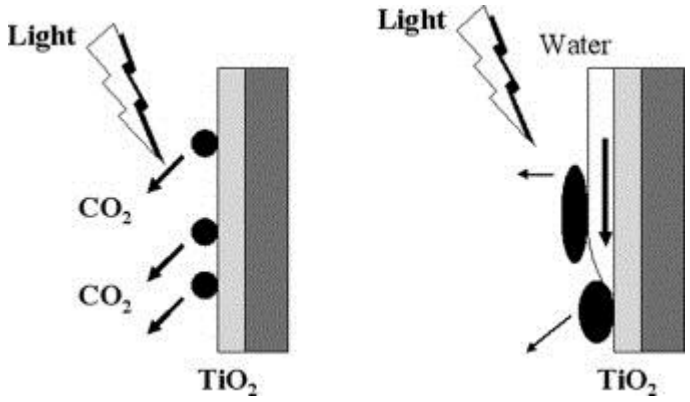

Figure 2.7 : Schematic diagram of the decomposition process in the self-cleaning surface [26].

TOTO Inc. is the main producer of TiO_2-based self- cleaning tiles in Japan. Its self-cleaning tiles have been applied on more than 5000 buildings in Japan according to statistical data for 2003. Among these, the most famous building is the Maru building, which lies in the central business district of Tokyo.

Figure 2.8 : The Shin Marunouchi Building in Tokyo.

Generally, the common tile covered building has to be cleaned every 5 years. How ever, the self-cleaning tiles are predicted to stay clean for more than 20 years by TOTO Inc., and thus save much of the cost for maintenance. In addition, self-cleaning tiles can decompose air pollutants such as nitrogen oxides (NOx), and reduce the amounts of detergents used; therefore, it is truly an environmentally benign construction material.

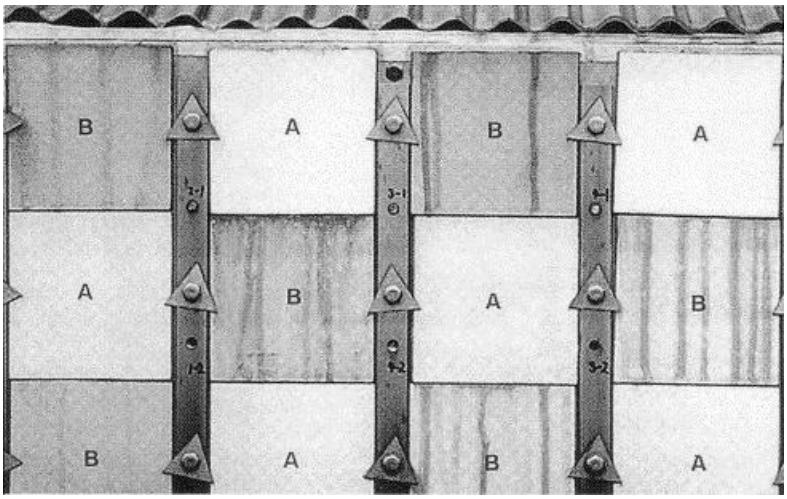

Figure 2.9 : . Photograph showing alternating self-cleaning (A) and ordinary (B) exterior wall tiles [31].

TiO_2 based self-cleaning glass is also an important commercial self-cleaning product. Such glass can maintain extreme visual clarity even on a rainy day, since water does not bead, but instead spreads evenly across the surface. If the amount of water is relatively small, the water layer becomes very thin and evaporates quickly. If the amount of water is larger, it forms a sheet like layer that also has high visual clarity. It may be surprising that TiO_2 coated glass can maintain the light transmittance properties of common glass, since the higher refractive index of TiO_2 enhances the surface reflection. Actually, TiO_2 nanoparticles are dispersed in a SiO_2 matrix in the coating for self-cleaning glass. The composition of the coating is carefully controlled so that its refractive index is close to that of glass.

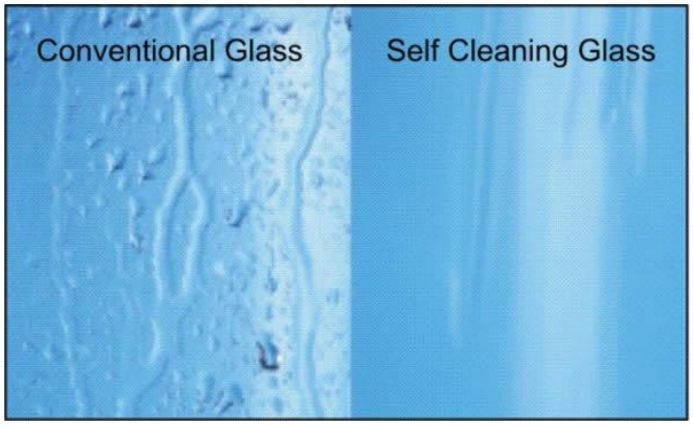

Figure 2.10 : Comparison between conventional glass and self cleaning glass.

Another important application of TiO_2 photocatalysts is in the purification of indoor air. Malodorous substances such as ammonia, hydrogen sulfide, acetaldehyde, toluene, methylmercaptan, etc., involve serious risks to health or comfort. Their concentrations in indoor air are always low, which is very suitable for TiO_2 based air purification. A photocatalyst type air cleaner is typically composed of TiO_2 based filters, UV lamps, and a fan for air circulation. The filters feature honeycomb-type construction or three-dimensional porous structure for minimum pressure drop. Fig. 9 shows a picture of TiO_2 coated porous ceramics filters for air cleaner uses.

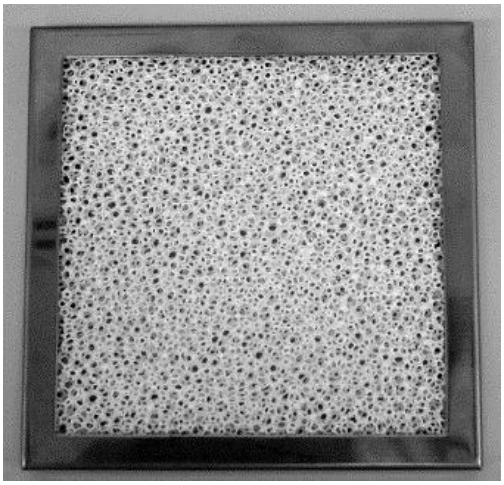

Figure 2.11 : Image of TiO_2 based ceramic filter for air purification application [26].

TiO_2 nanoparticles are coated on or dispersed in the body of filters with active carbon, zeolite, etc., as co-adsorbents. In contrast to the single function of adsorption for active carbon filters in conventional air cleaners, the TiO_2 based photocatalyst filter can decompose the adsorbed pollutants instead of accumulating them, and thus it exhibits better air- cleaning performance, as shown in Fig. 10. In addition, the photocatalyst type air cleaner can also kill the bacteria floating in indoor air, which is very important for the applications in hospitals, institutions for the elderly, and schools, etc.

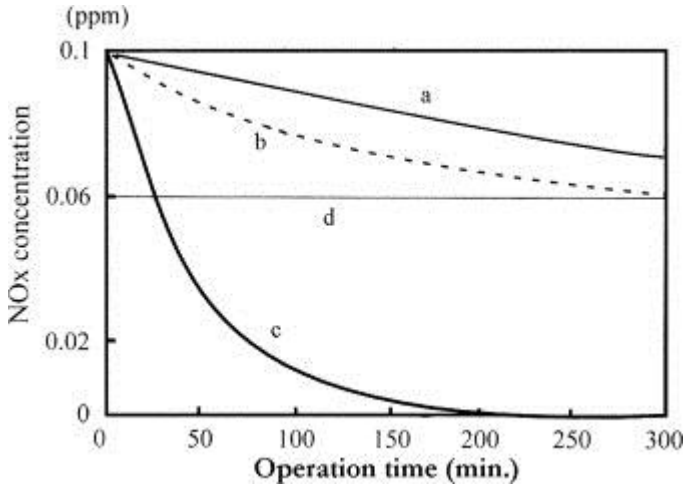

Figure 2.12 : Example of cleaning nitrogen oxide (NOx) in a typical apartment room. Curve a: natural decrease of NOx in room; curve b: NOx concentration change when an air cleaner containing only activated carbon adsorbent was working; curve c: NOx concentration change when an air cleaner containing irradiated photocatalyst on activated carbon was working; curve d: environmental standard for NOx (data courtesy of Daikin Industries, Ltd.) [26].

2.3.5 Why TiO_2 is the best photocatalyst?

The absorption of photons by a semiconductor provokes photocatalytic reactions at its surface, for example, water splitting or the degradation of organic compounds. As compared to other semiconductor photocatalysts, titanium dioxide has so far been shown to be the most promising material used for both fundamental research and practical applications, because it exhibits a higher photoreactivity (usually up to ζ (photonic efficiency) = 10%) and it is cheap, nontoxic, chemically and biologically inert, and photostable [32].

2.4 Methods of TiO_2 Preparation

Titanium dioxide is obtained either from minerals or from a solution of titanium salts or alkoxides. There are many synthetic methods for the preparation of TiO_2, a wide variety of approaches including flame synthesis, ultrasonic irradiation, chemical vapor deposition, as well as sol–gel reactions have been reported.

2.4.1 Overview of sol-gel process

Sol-gel processing is a wet chemical synthesis approach that generates inorganic oxides via gelation, precipitation or hydrothermal treatment.

Moreover, this method allows the shaping of the material (film, fiber and matrix) during the viscous sol step. It will be also possible to optimize the texture characteristics of the material by using the parameters controlling the polymerization kinetics. It is thus possible to prepare entirely new materials. The application of sol-gel technique is gaining interest basically due to several advantages including; good homogeneity, ease of chemical composition control, low processing temperature, large area coatings, low equipment cost, and good photocatalytic properties [34].

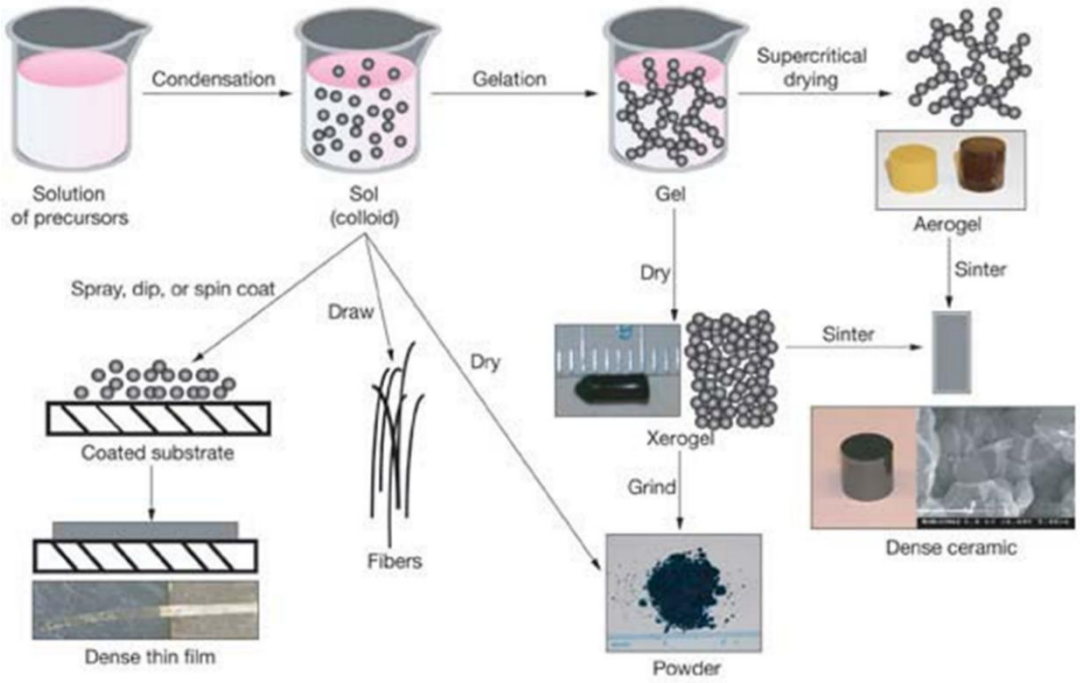

Figure 2.13 : Overview of the sol-gel process.

2.4.2 Precursors of sol-gel process

Several types of materials such as precursor of source material, solvent, catalyst, hydrolyzer and many other are used in sol-gel process.

2.4.2.1 Starting material

The best starting materials for sol-gel process are the class of materials known as metal alkoxides since these materials can react with water readily which is called hydrolysis. [33]. All metals form alkoxides and they have the $M(OR)_x$ general formula, where M is the metal, R is an alkyl group, and x is the valence state of the metal. Additionally, metal salt can be used in sol-gel process as starting materials. The most important starting materials which are used in sol-gel process are listed below.

Table 2.3 : Starting materials using in sol-gel process.

Material	Type	Application in sol-gel process
Titanium tetraisopropoxide	Metal alkoxide	TiO_2
TEOS	Metal alkoxide	SiO_2
Zinc acetate	Metal salt	ZnO

2.4.2.2 Solvent

Generally alcohols such as ethanol, methanol and 2-propanol are used in sol-gel process but using of THF, dioxane, formamide and DMF were reported [34]. The effect of using non alcoholic solvents in sol-gel derived SiO_2 particles was investigated

2.4.2.3 Catalyst

Different types of catalyst can be used in sol-gel process. Generally, HCl, ammonia and DMF were reported in sol-gel process as acid, base and nucleophilic type catalyst, respectively. The effect of catalyst nature and concentration was studied in our previous study [35].

2.4.3 The process parameters of sol-gel method

Various parameters are effective in sol-gel process and the characteristic and properties of the final product is dependant to these parameters. The most important parameters of sol-gel process are summarized below:

- ✓ The sol recipe
- ✓ Aging time
- ✓ Aging temperature
- ✓ Drying temperature and time
- ✓ Annealing temperature and time
- ✓ Advantages and disadvantages of sol-gel process

The advantages of sol-gel process are listed below [36].

- ✓ It uses relatively low temperatures.
- ✓ It can create very fine powders.

- ✓ It produces compositions not possible by solid-state fusion.

There are some disadvantages of the sol–gel process that are listed below [36].

- ✓ The cost of the raw materials (the chemicals) may be high.
- ✓ There is often large volume shrinkage and cracking during drying (we have to remove the “organics”).
- ✓ Organic chemistry often uses confusing terminology and is avoided by ceramists whenever possible.

3. PREPARATION OF MODIFIED TIO_2

TiO_2 shows relatively high reactivity and chemical stability under ultraviolet light ($\lambda<387nm$), whose energy exceeds the band gap of 3.3 eV in the anatase crystalline phase. The development of photocatalysts exhibiting high reactivity under visible light ($\lambda> 400$ nm) should allow the main part of the solar spectrum, even under poor illumination of interior lighting, to be used.

Several approaches for TiO_2 modification have been proposed:

- Metal-ion implanted TiO_2 (using transition metals: Cu, Co, Ni, Cr, Mn, Mo, Nb, V, Fe, Ru, Au, Ag, Pt) [37-39]
- Reduced TiOx photocatalysts
- Non-metal doped-TiO_2 (N, S, C, B, P, I, F)[40-42]
- Composites of TiO_2 with semiconductor having lower band gap energy (e.g. CdS particles [43]
- Sensitizing of TiO_2 with dyes (e.g. thionine)[44]
- TiO_2 doped with upconversion luminescence agent [45, 46]

3.1 Doping of TiO_2

3.1.1 General mechanism of doping

The visible light photoactivity of metal-doped TiO_2 can be explained by a new energy level produced in the band gap of TiO_2 by the dispersion of metal nanoparticles in the TiO_2 matrix. As shown in Fig. (1) electron can be excited from the defect state to the TiO_2 conduction band by photon with energy equals hv_2. Additional benefit of transition metal doping is the improved trapping of electrons to inhibit electron-hole recombination during irradiation. Decrease of charge carriers recombination results in enhanced photoactivity.

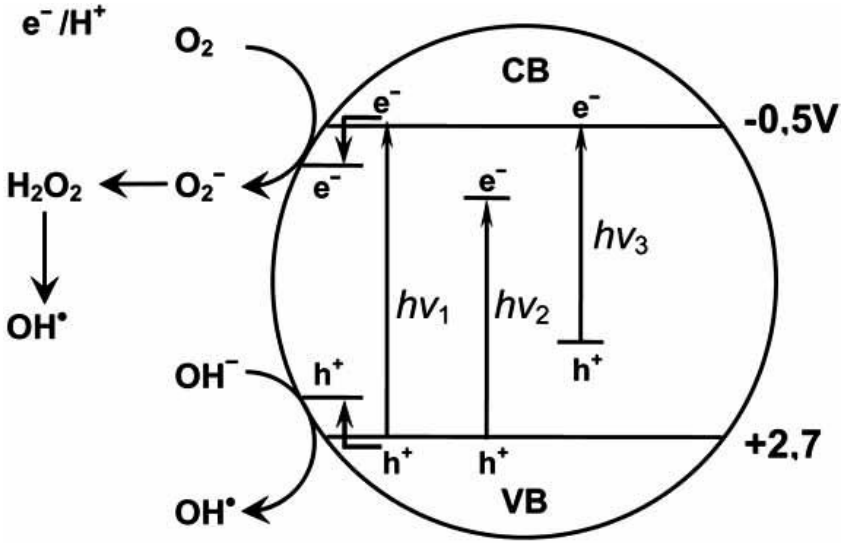

Figure 3.1 : Influence of doping on energy states of a semiconductor.

There are three different main opinions regarding modification mechanism of TiO_2 doped with nonmetals. (1) Band gap narrowing; (2) Impurity energy levels; and (3) Oxygen vacancies.

Band gap narrowing: Asashi, et al. found N 2p state hybrids with O 2p states in anatase TiO_2 doped with nitrogen because their energies are very close, and thus the band gap of N-TiO_2 is narrowed and able to absorb visible light [47].

Impurity energy level: Irie, et al. stated that TiO_2 oxygen sites substituted by nitrogen atom form isolated impurity energy levels above the valence band. Irradiation with UV light excites electrons in both the VB and the impurity energy levels, but illumination with visible light only excites electrons in the impurity energy level [48].

Oxygen vacancies: Ihara, et al. [20] concluded that oxygen-deficient sites formed in the grain boundaries are important to emerge vis-activity and nitrogen doped in part of oxygen-deficient sites are important as a blocker for reoxidation[49].

The modification mechanism of anatase doped with nonmetals was also analyzed by Zhao et al. They investigated N-TiO_2 and concluded that TiO_2 doped with substitutional nitrogen has shallow acceptor states above the valence state. In contrast, TiO_2 doped with interstitial nitrogen has isolated impurity states in the middle of the band gap. These impurity energy levels are mainly hybridized by N 2p states and O 2p states [50].

3.1.2 Methods for TiO_2 doping

To enhance the photocatalytic effect in the visible light region, many producing methods were proposed to dope (or incorporate) trace impurity in TiO_2 including: ion-assisted sputtering, plasma, ion-implantation, chemical vapor deposition (CVD) and sol-gel. A comprehensive list of doped TiO2 and methods of its preparation are shown in Table 1 [22-33].

3.1.3 Nitrogen doping of TiO_2

First non-metal doped TiO_2 was described in 1986 by Sato, et al.They obtained N-TiO_2 powders from a commercial titanium hydroxide by calcination. The powders showed higher photocatalytic activity for oxidation of carbon monoxide and ethane than standard TiO_2 in the visible region (434 nm). But at that time, this result did not attract attention. Only in 2001, Asashi, et al. reported the band-gap narrowing of titanium dioxide by nitrogen doping [18]. They prepared $TiO_{2-x}N_x$ films by sputtering the TiO_2 target in a N_2(40%)/Ar gas mixture and by treating anatase powder (ST01, Ishihara Sangyo Kaisha, Japan) in the NH3(67%)/Ar atmosphere at 600°C for 3 h [51].

3.1.4 Iron doping of TiO_2

The iron-doped-TiO_2 was prepared by the hydrothermal method. Titanium (IV) tetra-tert-butoxide and $FeCl_3$ or $FeCl_2$ dissolved in n-octanol was heated at 230°C for 2h in the presence of water. Resulting powders were rinsed, dried and calcined at 560°C. Photocatalyst doped with $FeCl_3$ have better photoactivity for degradation of dye in aqueous solution under UV and visible light. It was found that the amount of doped iron ions plays a significant role in affecting its photocatalytic activity [52].

3.1.5 Silver doping of TiO_2

Silver nitrate was mixed with reduction agent (sodium citrate tribasic dihydrate) and the reaction temperature was raised to 80°C with continuous stirring. Then TIP and HNO_3 were added and the reaction was maintained at 50°C for 24 h. The prepared sol was dried at 105°C for 24 h and calcined at 300°C [53].

3.1.6 co-doping of TiO_2

Nonmetal doping brings the serious problem of massive charge carrier recombination, which largely limits the photo-activity of doped TiO_2 under visible light [54]. Another inherent problem of the current nonmetal-doped TiO_2 photo-catalysts is that they gradually lose their photo-catalytic capability due to deactivation after illumination [55]. Thus, some researchers have investigated metal and nonmetal co-doping TiO2 such as N-Fe co-doping.

3.1.6.1 Nitrogen-iron co-doping of TiO_2

Recently, N-Fe co-doped TiO_2 have been prepared via several methods such as sol gel, hydrothermal and sono-chemical method [56-61] and proposed that co-doped samples exhibit higher photo-catalytic activity due to the new energy level formation [26-28]. To the best of our knowledge, a few reports are published on synthesis of N-Fe co-doped TiO_2 by sol-gel process using iron nitrate as iron source and urea as nitrogen source. Jian-Wei Fan et al. synthesized N-Fe co-doped TiO_2 via sol-gel method and used $Fe(NO3)_3$ as iron source and urea ($CO(NH_2)_2$) as nitrogen source [59]. They have prepared and characterized one sample, which has been doped with (0.5% of Fe, molar ratio) and (1.2% of N, molar ratio) anatase TiO_2 particles. But no study was reported about the dopants ratio effect films on structure and optical properties of N-Fe co-doped TiO_2.

In our study, pure TiO_2 and three N-Fe doped TiO_2 films with different nitrogen and iron dopant concentration were prepared and the effect of dopants ratio on crystal structure, microstructure, surface morphology and optical properties was investigated.

3.2 Silver Decorating of TiO_2

In particular, noble-metal nanoparticles (NPs) such as Au NPs [62] or Ag NPs [63] exhibit an improved response in the visible light region due to the effect of localized surface plasmon resonance (LSPR), produced by the collective oscillations of the surface electrons [64]. This is promising for extending the light absorption of TiO_2 into the visible range. Lu et al. [65] prepared the TiO_2/Au NPs photocatalyst by infiltrating Au NPs into TiO_2 photonic crystals and text results indicated that the photocatalytic activity of TiO_2/Au NPs was higher than that of unmodified TiO_2.

Another benefit of noble-metal NPs modification could be a reduction in the photo-generated charge carrier recombination. Tian et al. [66] reported that enhanced charge separation in the TiO_2/Au NPs was accomplished by the transfer of photoexcited electrons from the gold particle to the TiO_2 conduction band.

Ag NPs are of great importance due to their desirable strong resonance wavelength of 300–1200 nm but also because they are less costly than other noble metals [67]. These advantages make Ag NPs a good candidate for modification of TiO_2 NTAs, enhancing the visible light absorption and reducing the recombination rate of photogenerated charge carrier in TiO_2 NTAs. The Ag NPs decorated TiO_2 NTAs (Ag/TiO_2 NTAs) have been widely studied for use in photoelectrochemistry and photocatalysis [63, 68, 69].

3.3 TiO_2 Composites

The photoactivity of TiO_2 has been shown to be dependent on several key properties: crystal phase, surface area, exposed crystal facets, uncoordinated surface sites, defects in the lattice, and degree of crystallinity. Morphology control of TiO_2 via synthesis of composite materials has allowed for the improvement and fine-tuning of many of these properties. Additionally, TiO_2 composite structures can create and tune other properties such as mid-band-gap electronic states, which can alter charge migration or produce a red shift in the absorption spectrum.

Further, formation of heterojunctions between TiO_2 and other materials can yield visible light absorption by the added material with charge separation facilitated by the TiO2. The two main polymorphs of TiO_2 which show the highest photoactivity are the anatase and rutile phases, which have typically reported band-gap values of 3.2 and 3.0 eV, respectively. Although the band gap of rutile is narrower, the anatase phase is typically considered more favorable as it has a higher reduction potential and a slower rate of recombination of electron−hole pairs [7, 70]. Unfortunately, its wide band gap dictates that it will primarily absorb UV radiation. Here the utility of mixed phase TiO_2 must be discussed. Optimization and control of the phase transition and its applications have been covered in detail however, commercial Degussa P25, or simply P25 for short, is one of the most commonly used mixed phase TiO_2 composites.

This mixed phase material allows for utilization of visible light wavelengths through excitation of the rutile phase while also containing benefits of anatase TiO_2, such as a decreased recombination rate of charge carriers. The initial mechanism for this enhancement was ambiguous; however, utilizing electron paramagnetic resonance (EPR), Hurum et al. studied the fate of photogenerated charge carriers in order to shed light on the mechanism [71, 72]. They found that electrons which were photogenerated by the rutile component were transferred to a previously proposed electron trap site in the anatase lattice which lies 0.8 eV below the anatase conduction band [73].

Further, this is situated lower than the rutile conduction band. A decrease in electron−hole recombination is achieved since the photogenerated holes remain within the rutile component and the electrons are spatially separated into the anatase component. It was later determined that the photogenerated holes are preferentially trapped on the surfaces, whereas electrons become trapped within the lattice. As such surface electron trap sites increase the recombination rates, which indicates that a composite with a second material which is either a hole or an electron sink can further increase catalytic efficiency.

Beyond the use of mixed phase TiO_2, composites with non- TiO_2 materials are a very promising means to extend the usefulness of anatase into the visible wavelengths. Alternatively, for composites consisting of the rutile phase, inclusion of higher work function materials can yield slower charge carrier recombination. Other methods to decrease charge carrier recombination include increasing crystallinity, which can be done by high-temperature calcination, addition of dopants, or specific synthetic protocols. Additionally, defects, which can serve as charge carrier traps and reduce the recombination of photogenerated electron−hole pairs, can also be either induced or stabilized by formation of a composite. Composites which can help to tune the grain size have also been shown, such as metal oxide sol−gel precursors which can form composites with TiO_2 and inhibit crystallinity.

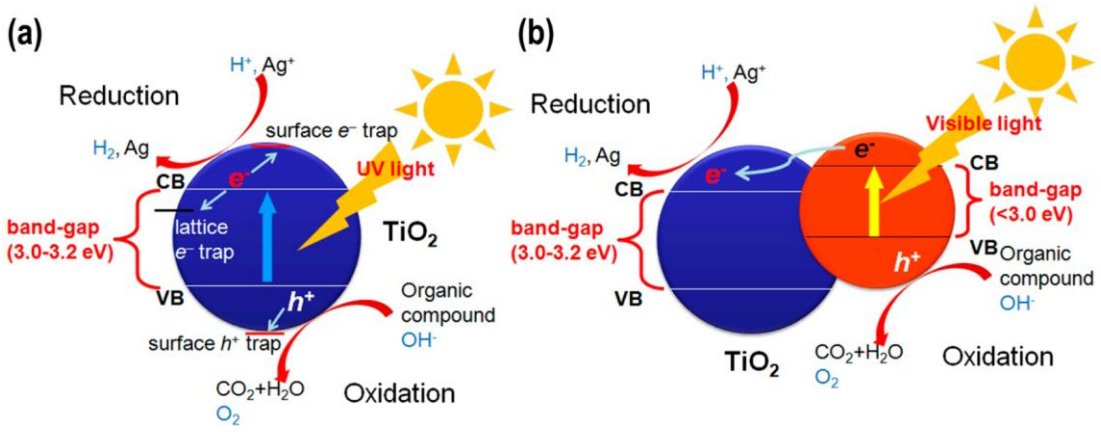

Figure 3.2 : Gerenal model for photocatalysis on anatase TiO_2.

Figure 1a shows a general model for photocatalysis on anatase TiO_2 in which light is absorbed to produce an electron−hole pair, charges migrate to the surface, and redox reactions occur. This ideal case assumes low charge recombination and easy charge migration to the surfaces. Charge separation can be enhanced by creation of features such as surface defects where electrons and holes can be trapped to prevent recombination or, as discussed earlier, in P25 where a natural electron trap exists below the anatase conduction band.

Figure 1b shows an improved case utilizing a TiO_2 composite heterojunction. In this case, a structure with a narrower band gap can utilize visible light to produce an electron−hole pair. Assuming a favorable band offset, the electron can migrate to the TiO_2, while the hole is trapped in the second material. Redox reactions are now free to occur at the separate surfaces since the likelihood of charge recombination has been diminished. A heterojunction composite structure can then be rationally designed in order to produce a favorable band offset and band positions in order to develop a catalyst for the needs of specific reactions, such as water splitting. In addition to the improvement of photocatalysis, composite structures can yield other benefits. Such advantages include the ability to tune the surface properties, i.e., acidity/basicity or open coordination sites, of the resultant materials, which is of importance to the adsorption of molecules, a critical factor relevant to catalysis, separation, and further modification.

Numerous mixed metal oxide/TiO_2 composites are beneficial for stabilization of thermal catalysts where reactions such as high-temperature NOx reduction are improved. Composites such as core−shell materials are also beneficial toward the stabilization of nanoparticles against phenomena such as sintering or aggregation.

Further, composites can be of great use to create highly porous materials, hollow shells, or hierarchical structures by templating methods.

4. EXPERIMENTAL

4.1 Materials

In this study, titanium tetraisoproproxide (TTIP) (SIGMA-ALDRICH 205273), 2-propanol (IPA) (MERCK 109634), hydrochloric acid fuming 37% (HCl) (MERCK 100317), urea (MERCK 108487), iron (III) nitrate nonahydrate (MERCK 103883), silver nitrate (MERCK 101512), silver nitrate aqueous solution (0.1N) (MERCK 109081), zinc acetate dihydrate (MERCK 108802), dietyhloamine (DEA) (SIGMA-ALDRICH 845028) were chemical pure and were used without any further purification.

4.2 Coating Method

All thin films were prepared by sol-gel dip-coating method. Soda-lime glass slides (25 mm × 75 mm in size and 1-1.2 mm in thickness) were phurchased from ISOLAB. TDC-10 dip-coater was used to coat slides and dipping-immersion speed can be adjusted from 50 $mm.min^{-1}$ to 250 $mm.min^{-1}$.

Figure 4.1 : Image of dip-coater.

4.3 Characterizations

XRD patterns were measured on a Rigaku using Cu-Kα radiation (λ=1.54 °A). The microstructure of the samples was investigated by FEI scanning electron microscopy. The thickness of the samples were calculated by Carl-Zeiss optical profilometer. The UV-Vis absorption spectra were obtained using Perkin Elmer spectrophotometer in

the range of 200-1100 nm. Infrared absorption spectra of the sample powders diluted with KBr were obtained with a spectrometer (Perkin-Elmer 1650FTIR) by the transmission method.

4.4 Preparation of Pure TiO_2 Thin Films

To the preparation of pure TiO_2 sample 2-propanol (IPA), hydrochloric acid fuming 37% (HCl) and titaniumtetraisopropoxide (TTIP) were used as solvent, catalyst and precursor, respectively. TTIP was dissolved in IPA and HCl under magnetic stirrer at 23 °C for 5 hours. The recipe of the sol is equal to my previous work [74] and was shown in table 4.1.

Table 4.1 : Optimized recipe of pure TiO_2 sol.

Precursor	Molar ratio
IPA	20
TTIP	1
HCl	0.1

Prepared sol was transparent, homogeneous and no precipitation was occurred. The image of the prepared pure TiO_2 sol is shown in Fig. 4.2. To the film preparation, the dipping and withdraw speed were fixed at 150 mm.min-1. Prepared film and sol were dried at 70°C for 2 hours and calcined at 450 °C (10°C/min) for 2 hours.

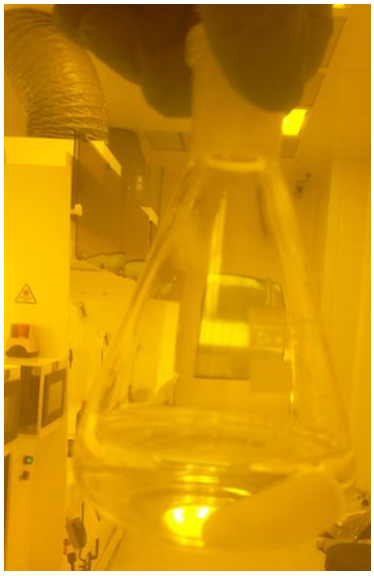

Figure 4.2 : Image of prepared pure TiO_2 sol.

4.5 Preparation of Pure TiO_2 Particles Using Different Catalyst Type And Concentration

Six TiO_2 sols with different catalyst type and catalyst concentration were prepared. The recipe was the same as previous section and only catalyst type and catalyst concentration were changed. The list of prepared samples is shown in table 4.2.

Table 4.2 : Prepared

Sample	Catalyst type	Catalyst	Catalyst molar ratio
H-1	Acid	HCl	0.1
H-2	Acid	HCl	1
D-1	Nucleophilic	DMF	0.1
D-2	Nucleophilic	DMF	1
A-1	Base	Ammonia	0.1
A-2	Base	Ammonia	1

4.6 Preparation of Doped TiO_2 (Thin) Films

To the preparation of doped TiO_2 sol, dopant source was added to pure TiO_2 sol before the stirring and all other parameters were fixed constant in all doped samples.

4.6.1 Nitrogen doped TiO_2 thin films

Urea was used as nitrogen dopant source and added to the sol with different concentrations. Dopant concentration is equal to weight percent of dopant source to to the sol. The list of prepared N-doped TiO_2 samples was shown in table 4.3.

Table 4.3 : Prepared N-doped TiO_2 samples.

Sample	Dopant Source	Dopant Concentration
N-1	Urea	1
N-2	Urea	2
N-3	Urea	3

Prepared sol was transparent, homogeneous and no precipitation was occurred. The image of prepared N-doped TiO_2 sol (N-1) is shown in Fig. 4.3.

Figure 4.3 : Image of prepared N-doped TiO_2 sol.

4.6.2 Iron doped TiO_2 thin films

Iron (III) nitrate was used as iron dopant source and was added to the sol with different concentrations. Dopant concentration is equal to weight percent of dopant source to to the sol. The list of prepared Fe-doped TiO_2 samples was shown in table 4.4.

Table 4.4 : Prepared Fe-doped TiO_2 samples.

Sample	Dopant Source	Dopant Concentration
F-1	$Fe(NO_3)_3$	1
F-2	$Fe(NO_3)_3$	2
F-3	$Fe(NO_3)_3$	3

Prepared sol was transparent, homogeneous and no precipitation was occurred. The image of prepared Fe-doped TiO_2 sol (F-3) is shown in Fig. 4.4.

Figure 4.4 : Image of prepared Fe-doped TiO_2 sol.

4.6.3 Silver doped TiO_2 thin films

Silver nitrate was used as silver dopant source and added to the sol with different concentrations. Dopant concentration is equal to weight percent of dopant source to to the sol. The list of prepared Ag-doped TiO_2 samples is shown in table 4.5.

Table 4.5 : Prepared Ag-doped TiO_2 samples.

Sample	Dopant Source	Dopant Concentration
AG-1	$AgNO_3$	0.5
AG-2	$AgNO_3$	1
AG-3	$AgNO_3$	0.25
AG-4	$AgNO_3$	0.75

Prepared sol that is shown in Fig. was transparent, homogeneous and no precipitation was occurred. Prepared sol was transparent, homogeneous and no precipitation was occurred. The image of prepared Ag-doped TiO_2 sol (F-3) is shown in Fig. 4.5.

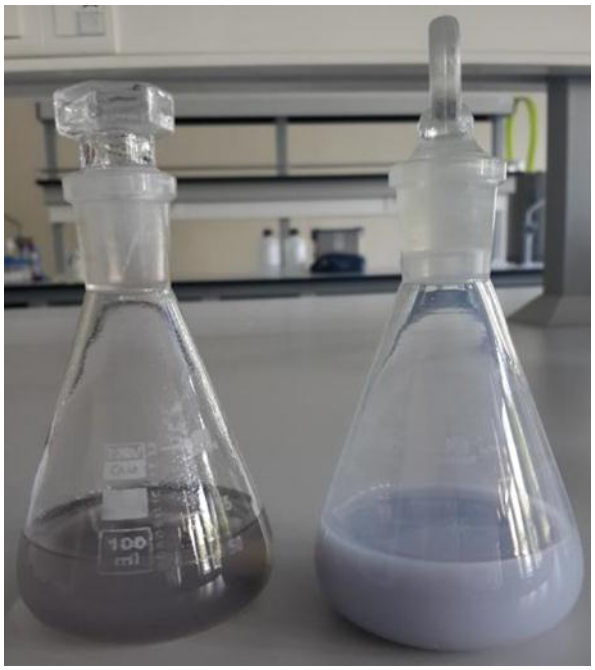

Figure 4.5 : Image of prepared Ag-doped TiO_2 sols.

4.6.4 Nitrogen-iron co-doped TiO_2 (thin) films

Urea and iron nitrate were used as nitrogen and iron dopant source, respectively and were added to the sol with different concentrations. The list of prepared N-Fe co-doped TiO_2 samples was shown in table 4.6.

Table 4.6 : Prepared N-Fe co-doped TiO_2 samples.

Sample	Urea Concentration	$Fe(NO_3)_3$ Concentration
CD-1	1.5	1.5
CD-2	2.5	0.5
CD-3	0.5	2.5

Prepared sol that was transparent, homogeneous and no precipitation was occurred.

4.7 Preparation of Silver Decorated TiO_2 Thin Films

Pure TiO_2 sols with previous recipe were prepared and coated on slides with 150 mm.min-1 dip-coating speed. The coated films were dried at room temperature for two days. Silver nitrate solution (0.1N) was used as silver source. Silver nitrate solution was coated on TiO_2 substrate by dip-coating method. Finally, several samples with different silver nitrate dip-coating parameter were prepared which are listed in table 4.7. The coated samples were dried at 100 °C and heated at 450 °C.

Table 4.7 : Prepared Ag decorated TiO_2 thin films.

Sample	Substrate	Dip-coating Speed	Heat Treatment Temperature
AGC-1	TiO_2	50	450 °C
AGC-2	TiO_2	150	450 °C
AGC-3	TiO_2	250	450 °C
AGC-4	TiO_2	150	120 °C

4.8 Preparation of TiO_2 @ ZnO Composite Thin Films

4.8.1 Pure ZnO thin film

To the preparation of ZnO sol, zinc acetate was firstly dissolved in methanol and Di-ethanolamin (DEA) solution at 50°C. The concentration of zinc acetate was kept at 0.3M and the weight ratio of DEA to zinc acetate was kept at 1.0. Then, the solution was aged for 24 hours at 50°C. Prepared sol that was transparent, homogeneous and no precipitation was occurred. The image of prepared pure ZnO sol was shown in Fig. 4.6.

Figure 4.6 : Image of prepared ZnO sol.

4.8.2 Preparation of TiO_2 @ ZnO composite thin films

Firstly, TiO_2 and ZnO sols were prepared separately as reported previously, then, two sols were mixed under magnetic stirrer for 2 hours with different TiO_2 to ZnO molar

ratio The list of prepared TiO_2 @ ZnO samples is shown in table 4.8. Finally, the slides were coated by dip-coating method with 150 mm.min-1 dipping speed.

Table 4.8 : Prepared TiO_2 @ ZnO composite samples.

Sample	Coated Material	TTIP : Zinc acetate (molar ratio)	Dip-coating Speed ($mm.min^{-1}$)
C-1	TiO_2@ZnO	1 : 1	150
C-2	TiO_2@ZnO	2 : 1	150
C-3	TiO_2@ZnO	1 : 2	150

5. RESULTS AND DISCUSSION

5.1 Effect of Catalyst Nature And Concentration on TiO_2 Particles

The XRD technique was used to identify the phases of the samples and its patterns are shown in Fig. 5.1 which confirms anatase structure in H-1, H-2, A-1, A-2, P-5 and amorphous structure in P-3. The amorphous structure of P-6 sample is due to the high concentration of basic catalyst and it is related to the basic hydrolysis and polymerization mechanism and kinetics.

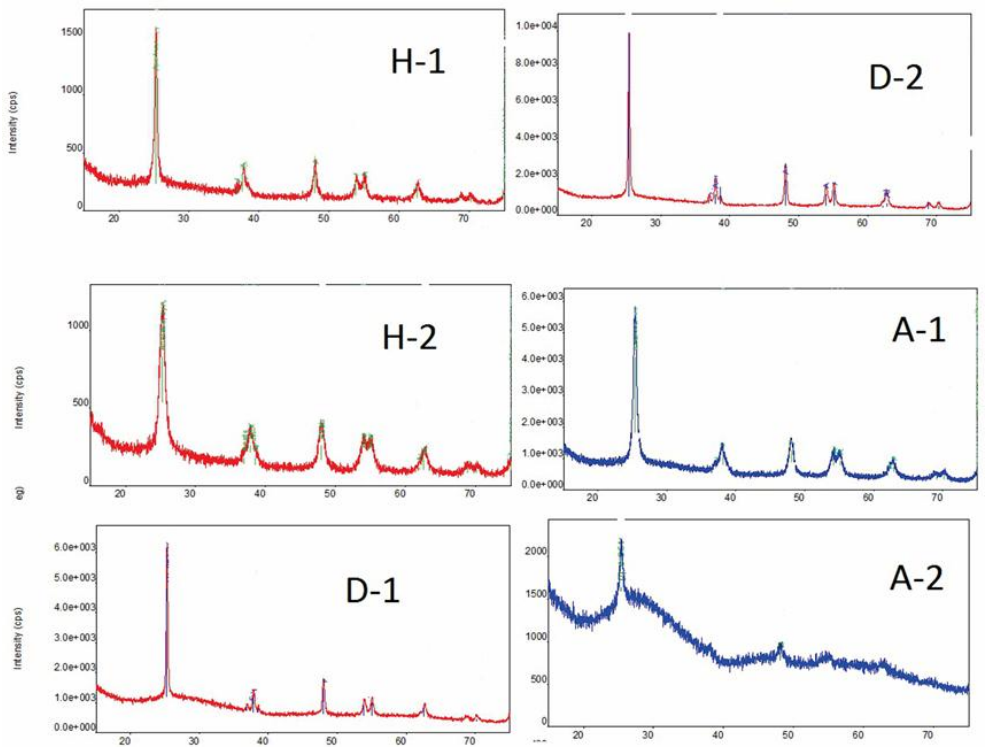

Figure 5.1 : XRD patterns of TiO_2 particles prepared by different catalyst type and concentration

The crystallite size of the samples is shown in table 5.1.

Table 5.1 : Average crystalline size of samples prepared by different catalyst type and concentration.

Sample	Catalyst	Catalyst concentration	Crystal structure	2θ (degree)	FWHM (degree)	Average crystallite size (nm)
H-1	HCl	0.1	Anatase	25.252	0.384	16
H-2	HCl	1	Anatase	25.277	0.903	6
D-1	DMF	0.1	Anatase	25.274	0.220	28
D-2	DMF	1	Anatase	25.346	0.226	27
A-5	NH_3	0.1	Anatase	25.329	0.555	11
A-6	NH_3	1	Amorphous	-	-	-

Samples prepared with DMF have narrower picks than samples prepared with HCl, which shows that samples prepared with acidic HCl catalyst, have smaller particle size. According to the XRD patterns of H-1 and H-2, by increasing of HCl concentration, it seems that the picks were broader and particle size decreases.

5.2 Pure TiO_2 Thin Films

5.2.1 Structural properties of pure TiO_2 thin films

The XRD pattern of sample P-2 which is optimized is shown in Fig. 5.2 which confirms the presence of the anatase crystal structure. The rutile peak is not seen at this samples.

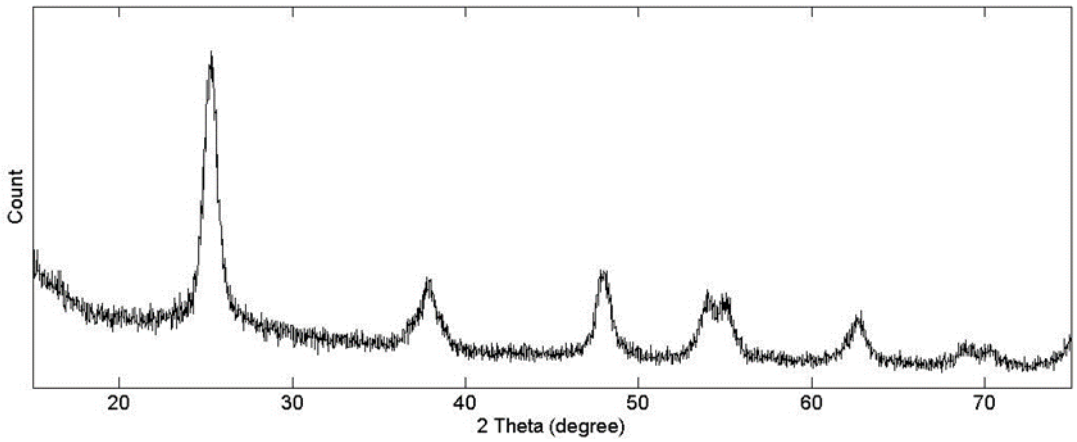

Figure 5.2 : XRD pattern of pure TiO_2.

As mentioned in previous section, the crystallite size of the P-2 sample was calculated using Scherrer equation and is shown in table 5.2.

Table 5.2 : Average crystalline size of pure TiO_2.

Sample	Crystal structure	2θ (degree)	FWHM (degree)	Average crystallite size (nm)
P-2	Anatase	25.277	0.903	6

The FT-IR pattern of the TiO_2 film was shown in Fig. 5.3. The absorption band at 500-600 cm-1 in both figures is due to the vibration of the Ti-O band in TiO_2 lattice. The absorption band appearing at 950 and 1020 cm-1 are representing the stretching vibration of the O-C-C of the TTIP isopropyl group and large absorption peaks in the region 3000-3600 cm-1 are related to the OH stretching frequencies of 2-propanol.

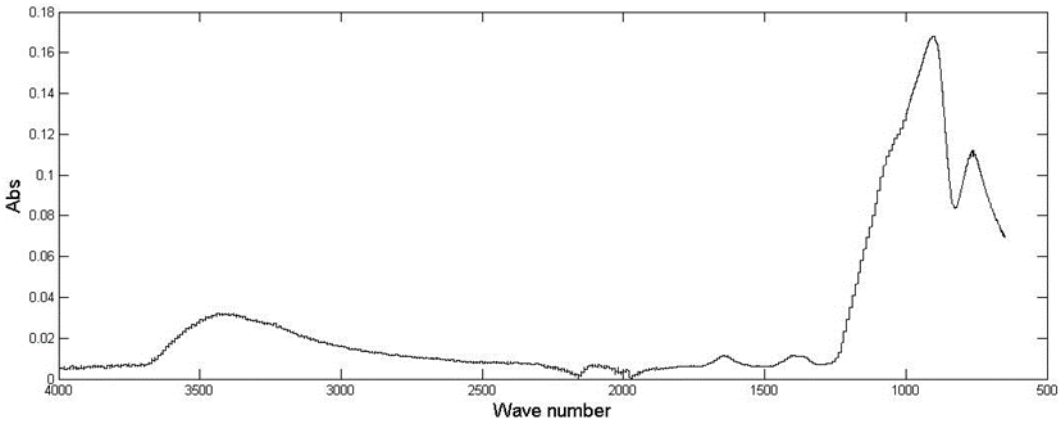

Figure 5.3 : FT-IR pattern of pure TiO_2 thin film

To the elemental characterization of the pure TiO_2 sample, EDS was used firstly. The EDS spectrum of the pure TiO_2 thin film was shown in Fig. 5.4 and the elemental composition of the pure TiO_2 which is taken from EDS spectrum is shown in table 5.3.

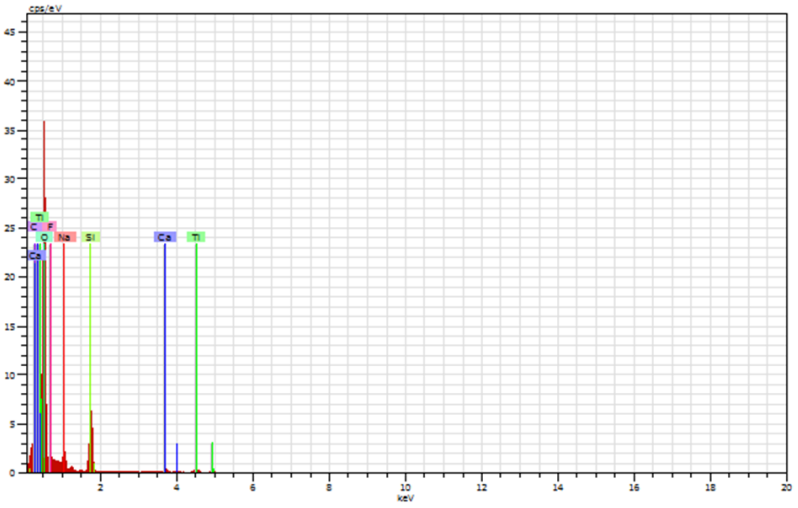

Figure 5.4 : EDS pattern of pure TiO_2 thin film.

The elemental composition taken from EDS shows very low amount of titanium element. It can be concluded that EDS is not a good approach to elemental characterization of prepared thin films and it measures the elemental composition of the soda-lime glass, which is our substrate.

Table 5.3 : Elemental composition of pure TiO_2 taken by EDS.

Element	Atomic number	Weight %	Atomic %
O	8	68.23	66.57
C	6	19.36	25.16
F	9	5.44	4.47
Si	14	4.23	2.35
Na	11	1.48	1
Ti	22	0.74	0.24
Ca	20	0.52	0.2
TOTAL		100	100

An XPS spectrum of pure TiO2 thin film is reported in Fig. 5.5 and the position of the Ti 2p3/2 peak (458 eV) is close to the reported value by reference and the oxidation level of titanium is +4 as expected.

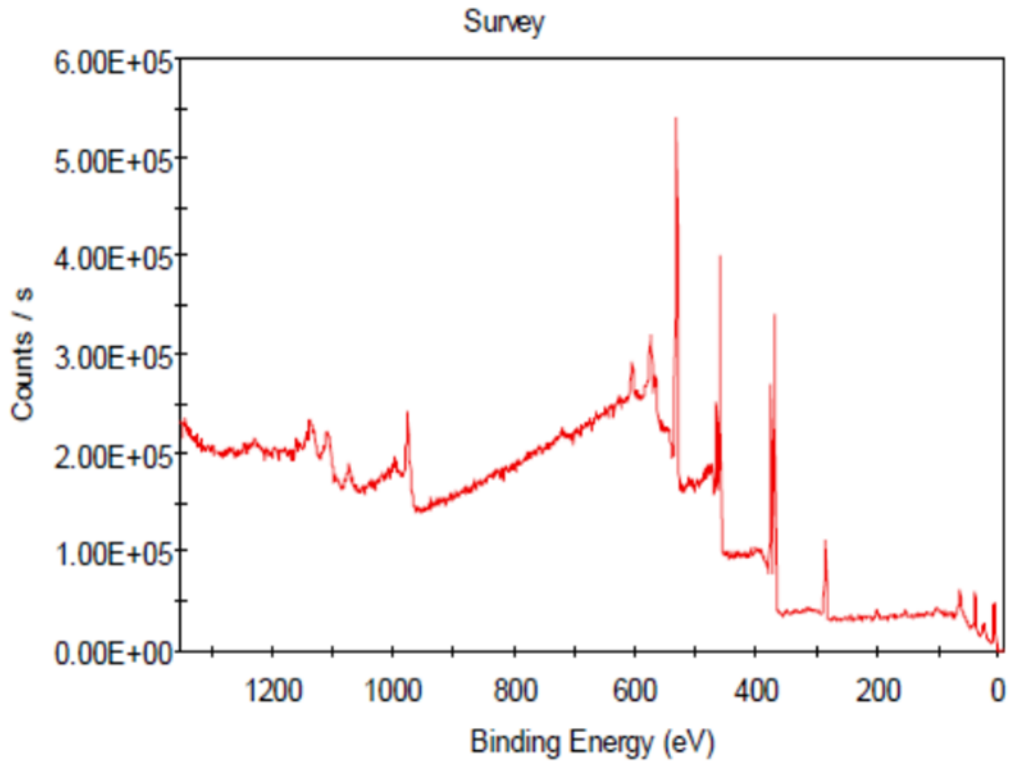

Figure 5.5 : XPS survey of pure TiO_2 thin film.

The surface elemental analysis of XPS is shown in table 5.4 and reveal the presence of titanium and oxygen element as expected. However, surprisingly carbon element was remained and it can be due to the low calcination time.

Table 5.4 : Elemental composition of pure TiO_2 thin film taken by XPS.

Element	Atomic %
Ti	24.27
O	61.79
C	13.95
TOTAL	100

The 3D surface topography of pure TiO_2 is shown in Fig. 5.6, which is taken by confocal microscopy. It is clear that the pure TiO_2 sample has a sharp edge between substrate and coating.

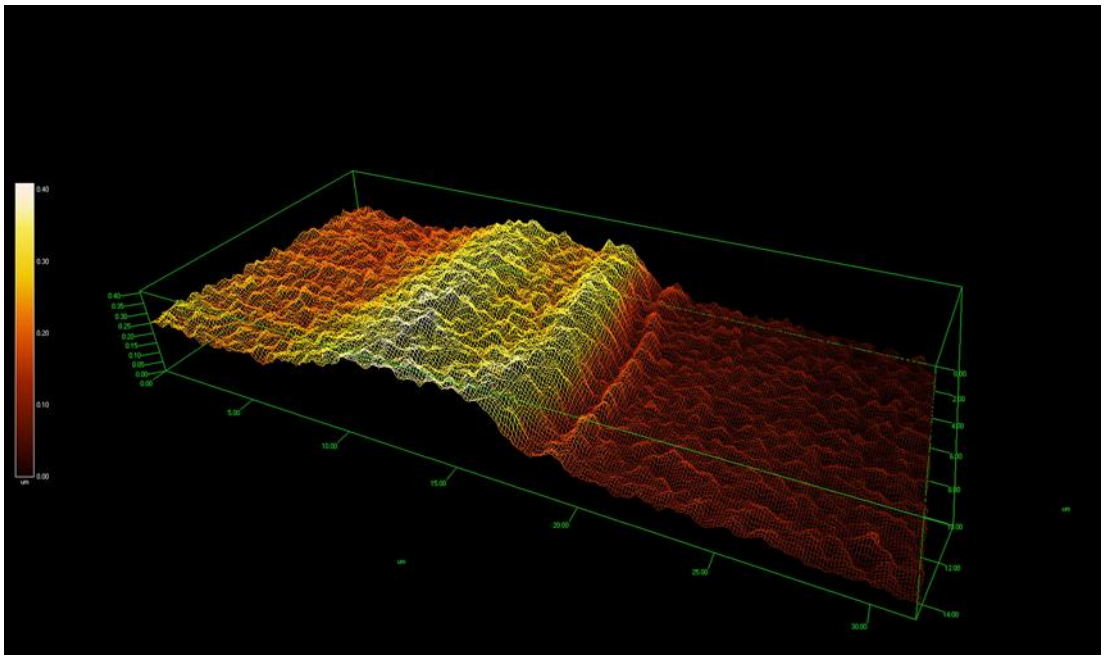

Figure 5.6 : 3D surface topography of pure TiO_2 taken by confocal microscopy

The SEM image of the prepared pure TiO_2 thin film is shown in Fig. 5.7. It was seen that pure TiO_2 sample has a homogeneous structure with a particle size between 20 nm and 30nm.

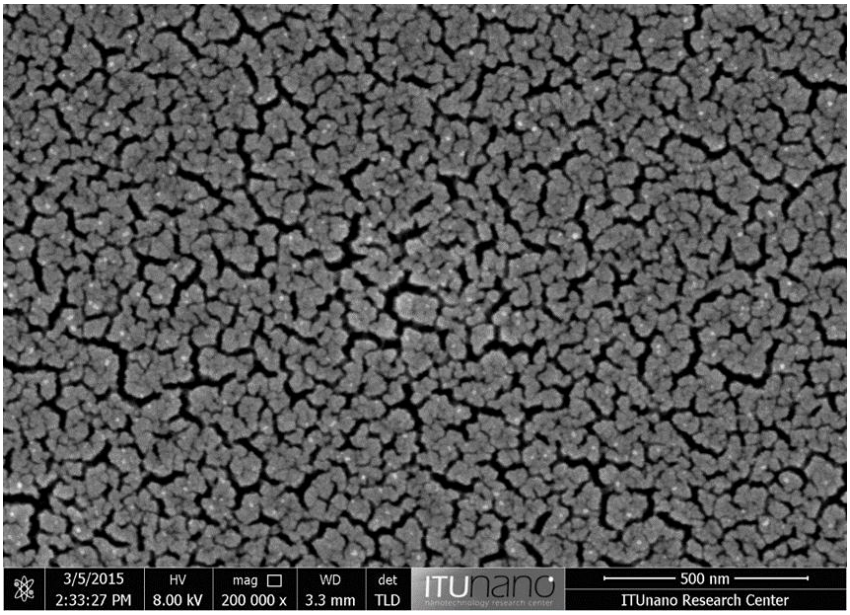

Figure 5.7 : SEM image of pure TiO_2 thin film.

5.2.2 Optical properties of pure TiO_2 thin film

The optical absorption spectrum of prepared pure TiO_2 is shown in Fig 5.8 and shows that the absorption edge of the pure TiO_2 sample is around 350 nm.

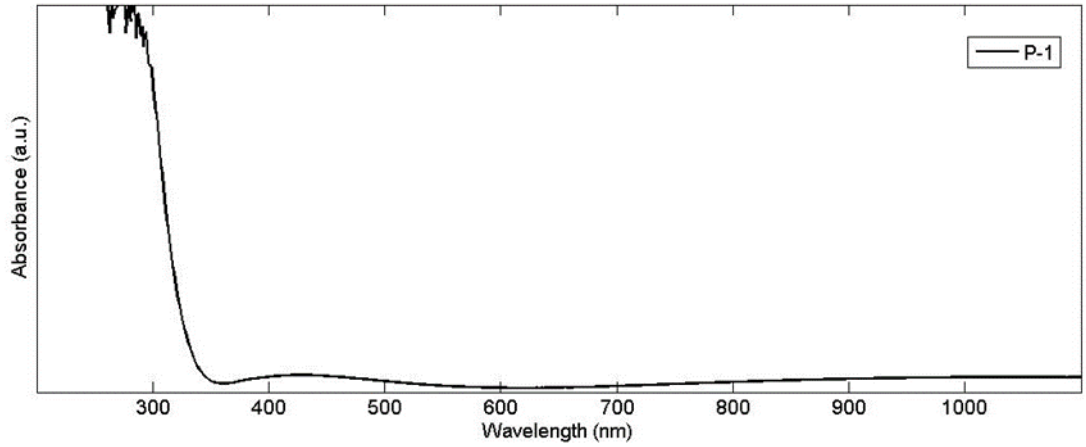

Figure 5.8 : UV-Vis optical absorption spectrum of pure TiO_2 thin film

The reflectance spectrum of prepared pure TiO_2 is shown in Fig. 5.9.

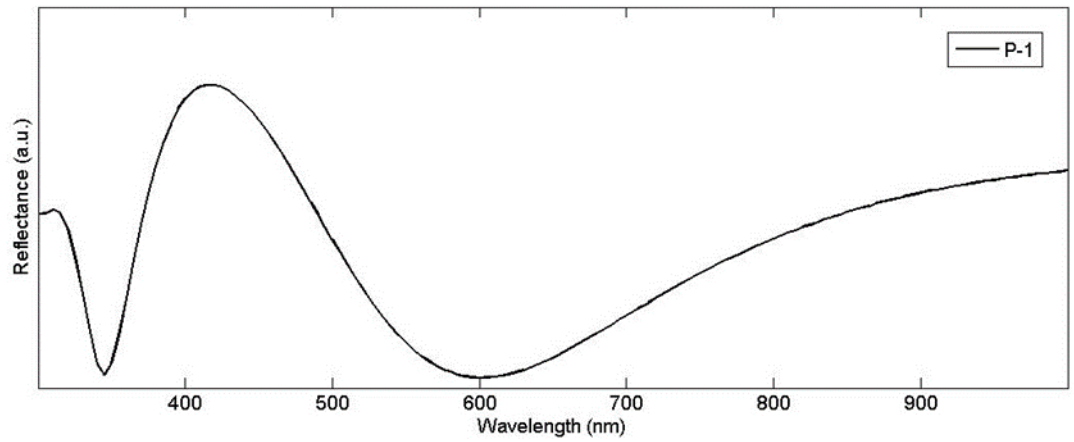

Figure 5.9 : UV-Vis optical reflectance spectrum of pure TiO_2 thin film.

The Tauc plot of prepared pure TiO_2 thin film is shown in Fig 5.10 and shows that the absorption edge of the prepared pure TiO_2 thin film is about 330 nm which is lower than reported anatase pure TiO_2; therefore the band gap value obtained is about 3.55 eV, which is higher than the reported band gap value for crystalline anatase TiO_2. The high band gap value of the prepared film may be due to the thermal stress

effects produced in the film [75]. This result is in agreement with the Welte et al [76].

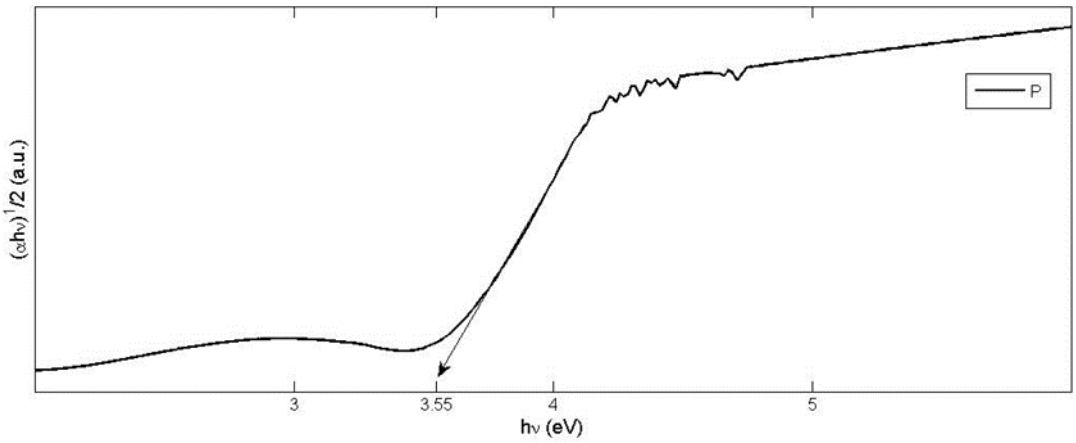

Figure 5.10 : Tauc plot of pure TiO_2 thin film.

5.3 Doped TiO_2 Thin Films

5.3.1 Nitrogen doped TiO_2 thin films

The optical absorbance of N-doped TiO_2 thin films are shown in Fig. 5.11 and state that the wavelength of the absorption edge does not increase by increasing the dopant concentration. The wavelengths of optical absorption edge of the N-doped TiO_2 thin films are shown in table 5.5 and show that the absorption edge of sample N-2 which doped with 1.5 wt% nitrogen relies on visible light region [77].

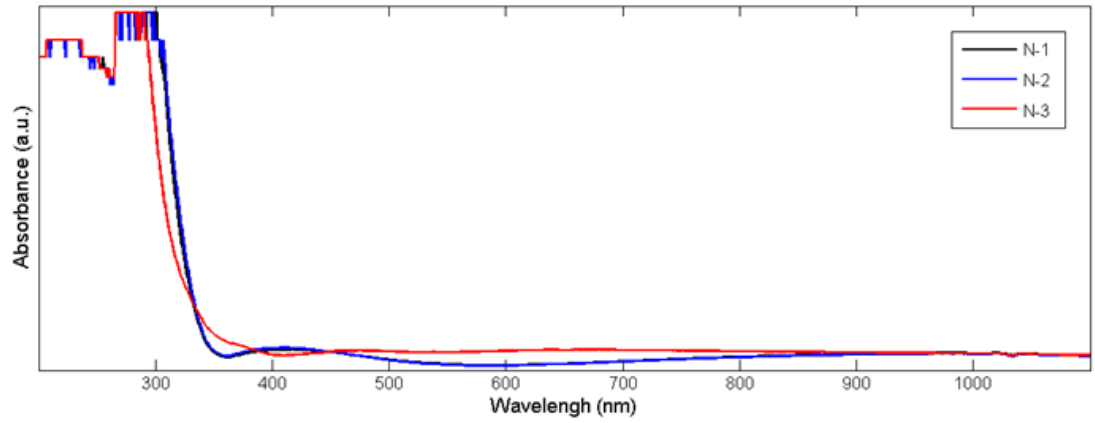

Figure 5.11 : UV-Vis absorption spectra of N-doped TiO_2 thin films.

Table 5.5 : Absorption edge of N-doped TiO_2 thin films.

Sample	Dopant	Dopant concentration (wt%)	Wavelength of absorption edge (nm)
N-1	Nitrogen	0.5	350
N-2	Nitrogen	1.5	355
N-3	Nitrogen	3	340

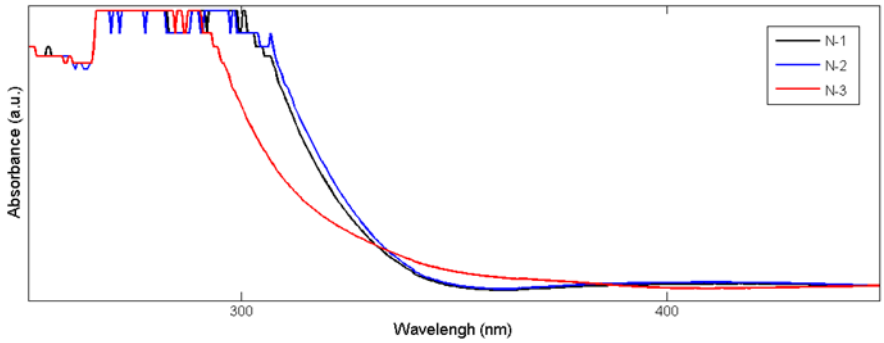

Figure 5.12 : Absorption edge shifting in N-doped TiO_2 thin films.

The Tauc plot of the N-doped TiO_2 samples are shown in Fig. 5.13 and propose that the lowest optical band-gap belongs to the sample N-2 which is doped with 1.5 wt% nitrogen. The calculated band-gap of the N-doped TiO_2 samples are listed in table 5.6.

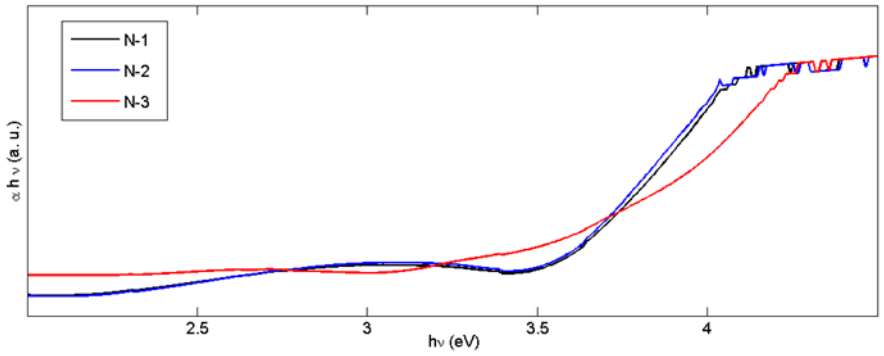

Figure 5.13 : Tauc plot of N-doped TiO_2 thin films.

Table 5.6 : Band-gap of N-doped TiO_2 thin films

Sample	Dopant	Dopant concentration (wt%)	Calculated E_g
N-1	Nitrogen	0.5	3.4
N-2	Nitrogen	1.5	3.35
N-3	Nitrogen	3	3.5

5.3.2 Iron doped TiO_2 thin films

The optical absorbance of Fe-doped TiO_2 thin films are shown in Fig. 5.14 and state that the wavelength of the absorption edge increases by increasing the dopant concentration. The wavelengths of optical absorption edge of the Fe-doped TiO_2 thin films are shown in table 5.7 and show that the absorption edge of sample F-3 which doped with 3 wt% iron relies on visible light region [77].

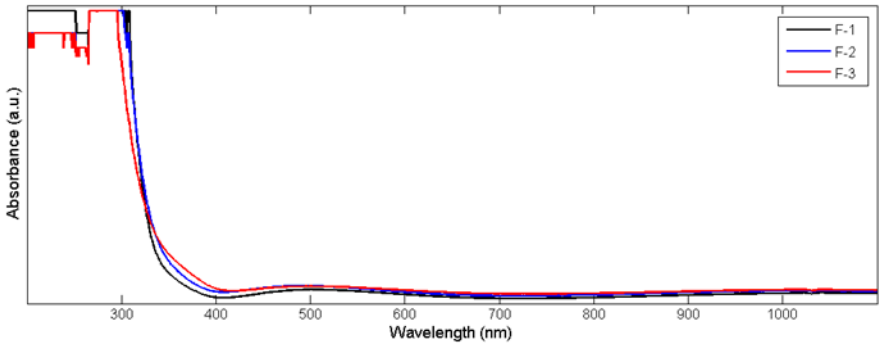

Figure 5.14 : UV-Vis Optical absorption of Fe-doped TiO_2 thin films.

Table 5.7 : Calculated band-gap of Fe-doped TiO_2 thin films.

Sample	Dopant	Dopant concentration (wt%)	Wavelength of absorption edge (nm)
F-1	Iron	0.5	340
F-2	Iron	1.5	350
F-3	Iron	3	370

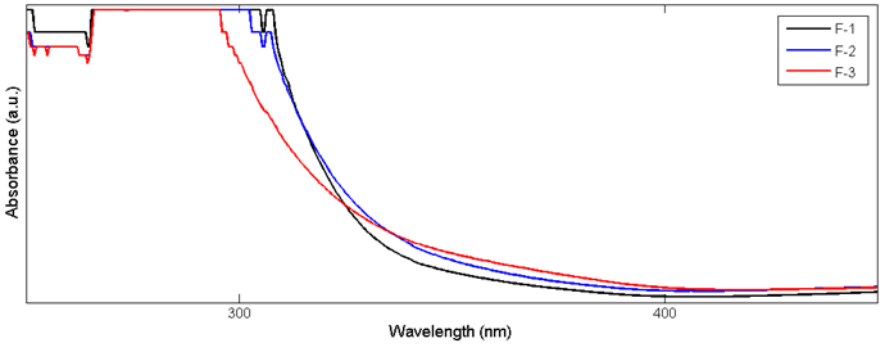

Figure 5.15 : Shifting of absorption edge in Fe-doped TiO_2 thin films.

The Tauc plot of the Fe-doped TiO_2 samples are shown in Fig. 5.16 and propose that the lowest optical band-gap belongs to the sample F-3 which is doped with 3 wt% iron. The calculated band-gap of the Fe-doped TiO_2 samples are listed in table 5.8.

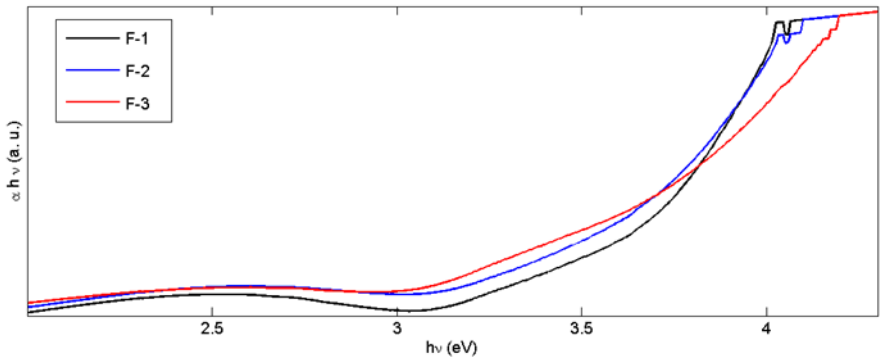

Figure 5.16 : Tauc plot of Fe-doped TiO_2 thin films.

Table 5.8 : Calculated band-gap of Fe-doped TiO_2 thin films.

Sample	Dopant	Dopant concentration (wt%)	Calculated E_g
F-1	Iron	0.5	3.5
F-2	Iron	1.5	3.4
F-3	Iron	3	3.1

5.3.3 Silver doped TiO_2

The optical absorbance of Ag-doped TiO_2 thin films are shown in Fig. 5.17 and state that the wavelength of the absorption edge does not increase by increasing the dopant concentration. The wavelengths of optical absorption edge of the Ag-doped TiO_2 thin films are shown in table 5.9 and show that the absorption edge of all silver doped samples relies on UV light region.

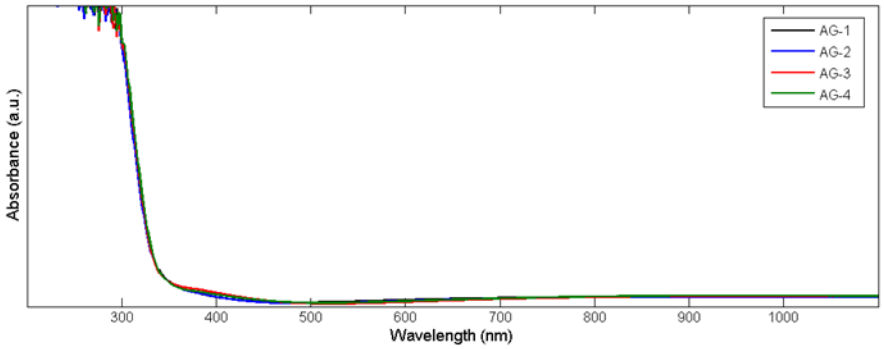

Figure 5.17 : UV-Vis optical absorption of Ag-doped TiO_2 thin films.

Table 5.9 : Absorption edge of Ag-doped TiO_2 thin films.

Sample	Dopant	Dopant concentration (wt%)	Wavelength of absorption edge (nm)
AG-1	Silver	0.5	340
AG-2	Silver	1	340
AG-3	Silver	0.25	340
AG-4	Silver	0.75	340

The Tauc plot of the Ag-doped TiO_2 samples were drawn and propose that the lowest optical band-gap belongs to the sample AG-3 which is doped with 0.25 wt% silver. The calculated band-gap of the Ag-doped TiO_2 samples are listed in table.

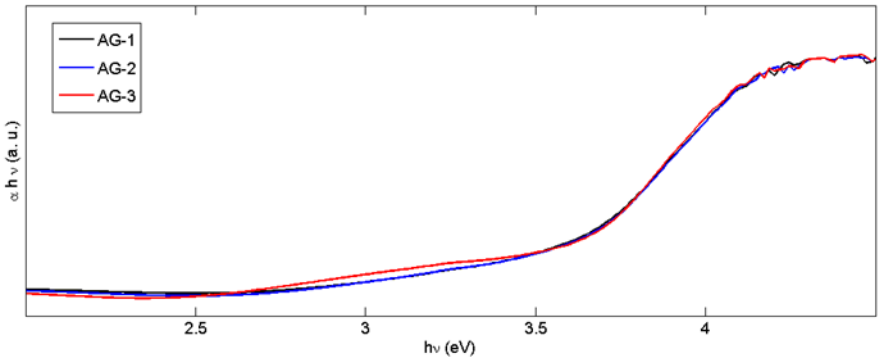

Figure 5.18 : Tauc plot of Ag-doped TiO_2 thin films.

Table 5.10 : Calculated band-gap of Ag-doped TiO_2 thin films.

Sample	Dopant	Dopant concentration (wt%)	Calculated E_g
AG-1	Silver	0.5	3.5
AG-2	Silver	1	3.5
AG-3	Silver	0.25	3.5
AG-4	Silver	0.75	3.5

5.3.4 Nitrogen-iron co-doped TiO_2 (thin) films

5.3.4.1 Structural properties of N-Fe co-doped TiO_2 (thin) films

The XRD patterns of the prepared powders are shown in Fig. 5.19, which shows that P and CD-3 samples have full anatase crystal structure. On the other hand, CD-1 and CD-2 samples have amorphous structure. Since the Fe^{3+} radius (0.064 nm) and N^{3+} (0.016 nm) were smaller than the Ti^{4+} radius (0.068 nm), they can penetrate into TiO_2 lattice. Sample with medium dopants concentration has amorphous structure and it may be attributed to the disordering of the TiO_2 lattice by the both iron and nitrogen atoms. Thus, the dopants ratio is important parameter on resulting crystal structure of N-Fe co-doped samples.

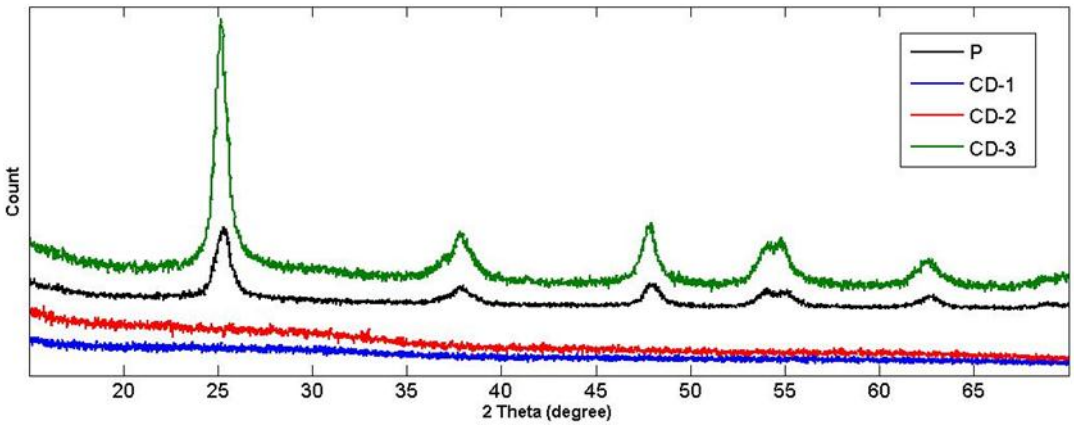

Figure 5.19 : XRD patterns of N-Fe co-doped TiO_2 (thin) films.

The particle characteristics and thickness of the samples are summarized in Table 5.11. The sample CD-3 has the smaller particle size in comparison with pure TiO_2 (P). In sample CD-3 which has lower dopants ratio, iron and nitrogen enter TiO_2

lattice but they can`t break the crystal structure and only inhibit the growth of the particle size.

Table 5.11 : Particle characteristics of pure and N-Fe co-doped TiO_2 films.

Sample	Crystal structure	2θ (degree)	FWHM (degree)	Average crystalline size (nm)
P	Anatase	25.277	0.38	10
CD-1	Amorphous	-	-	-
CD-2	Amorphous	-	-	-
CD-3	Anatase	25.153	0.714	6

The SEM images of the prepared samples are shown in Fig. 5.20. It is seen that pure TiO2 sample has a homogeneous structure with a particle size between 20 nm and 30nm. The microstructure of sample CD-3, which is transparent is similar to pure sample with a particle size between 25nm and 35nm. But, the microstructures of CD-1 and CD-2 samples are different from samples P and CD-3. In comparison with other samples, the CD-1 sample has much bigger and inhomogeneous particles up to 250nm. The CD-2, which has lower dopants ratio, has the particle size up to 100nm. However, CD-3 with dopants ratio of 33.62 has much smaller particle sizes in the range of 25 – 35 nm. Thus, dopants ratio could be an effect to control particle size of N-Fe co-doped TiO2. The transparency of the samples P and CD-3 may be related to the lower particle size too.

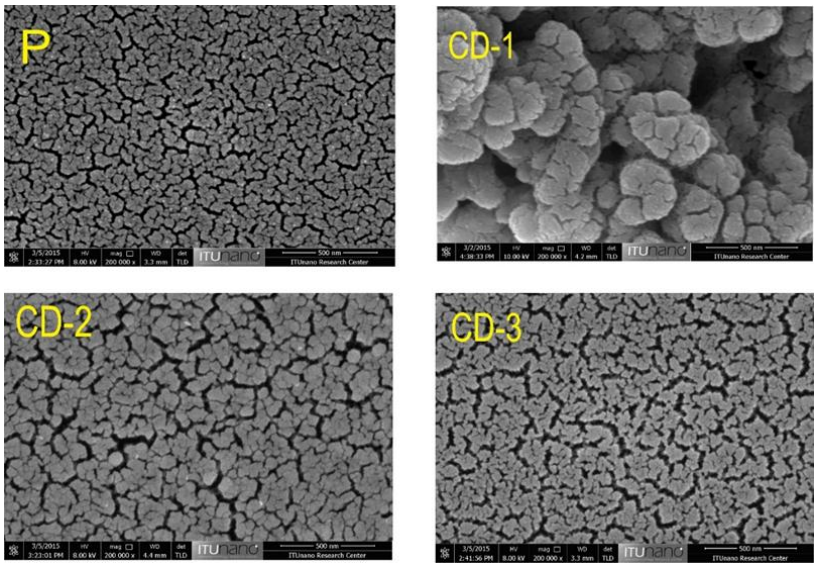

Figure 5.20 : SEM images of pure and N-Fe co-doped TiO_2 films.

The roughness average (Ra) and root mean squared value (RMS) are calculated according to the following equations:

$$R_a = \sqrt{\frac{\sum_{i=1}^{N}(Z_i - Z_{av})}{N}} \quad RMS = \sqrt{\frac{\sum_{i=1}^{N}(Z_i - Z_{av})^2}{N}}$$

where Zi, Zav and N are the height of individual point i, average height of the entire region and the number of points measured within a given area. The surface roughness parameters of the samples are shown in table 5.12. It is seen that the surface roughness is similar in the case of P and CD-2 samples, and the surface roughness is about 88 and 216 nm for CD-1 and CD-3 samples, respectively. Samples of P and CD-2 have relatively smooth surface but the surface of other films are much rougher.

Table 5.12 : Surface roughness parameters of pure and N-Fe co-doped TiO_2 films.

Sample	Roughness average (R_a) (nm)	Root mean squared (RMS) (nm)
P	9	1
CD-1	88	108
CD-2	10	12
CD-3	216	303

The 3D surface topography of the prepared films are shown In Fig. 5.21. It is clear that the samples with lower dopants ratio (P and CD-2) have sharp edge between substrate and coating. But the samples with high dopants ratio (CD-1 and CD-3) have no sharp edge between the substrate and coating. Especially the sample CD-3 has a rough edge and it may be attributed to the higher amount of iron concentration.

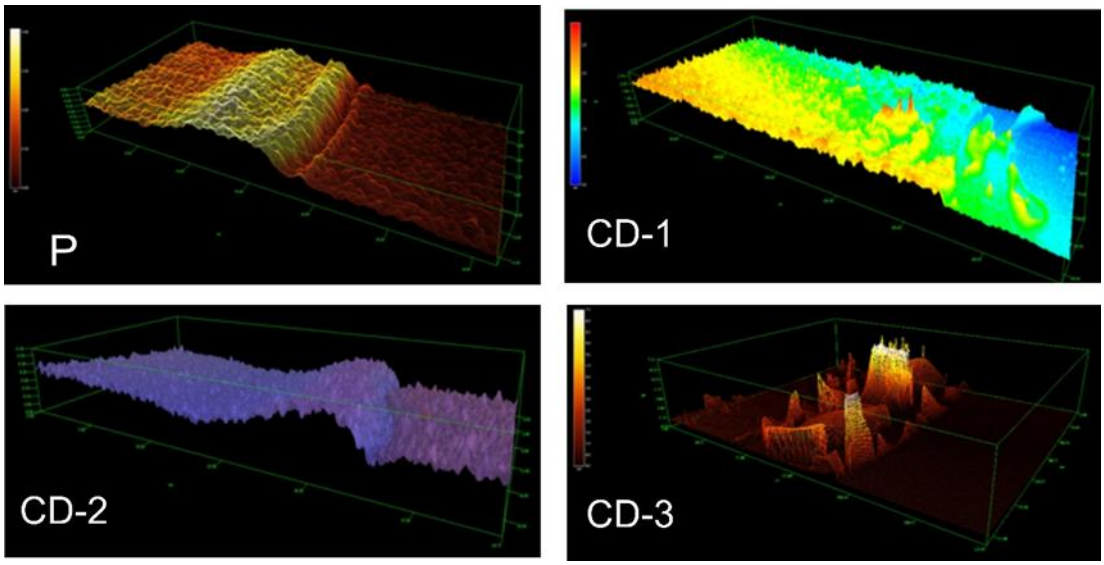

Figure 5.21 : 3D topography of pure and N-Fe co-doped TiO_2 films taken by confocal microscopy

5.3.4.2 Optical properties of N-Fe co-doped TiO_2

The absorption and transmission spectra of the samples are shown in Fig. 5.22 and Fig. 5.23, respectively. The transparency of the samples was shown in table 5.13. The P, CD-2 and CD-3 samples were transparent but CD-1 sample has become opaque in a short time after dip-coating. It may attributed to the change of fractal dimension during film formation in dip-coating process which has been investigated by Brinker et al [78]. The possible structures of the inorganic precursors range from weakly branched polymers to high condensed particles in sol-gel dip-coating process. In the case of fractal objects, the packing efficiency depends on the fractal dimension, size, and condensation rate. They reported that if each object has a fractal dimension less than 1.5, the probability of intersection decreases indefinitely as object radius (R) increases. These structures are mutually transparent during film formation, they freely interpenetrate as they are forced into close proximity by the increasing concentration. Alternatively, if the fractal dimension of each object exceeds 1.5, the probability of intersection increases algebraically with R, and their structure became porous and opaque.

It was found that these features of N-Fe co-doped TiO_2 can be obtained by changing the dopants ratio: a) Transparent anatase b) Opaque amorphous c) Opaque anatase

Table 5.13 : Transparency of pure and N-Fe co-doped TiO_2 films.

Sample	Iron nitrate/Urea (molar ratio)	Transparent/opaque	Crystal structure	Transparency (%) (@λ=500nm)
P	-	Transparent	Anatase	81.4
CD-1	6.72	Opaque	Amorphous	2.32
CD-2	1.34	Transparent	Amorphous	59.8
CD-3	33.62	Transparent	Anatase	74.9

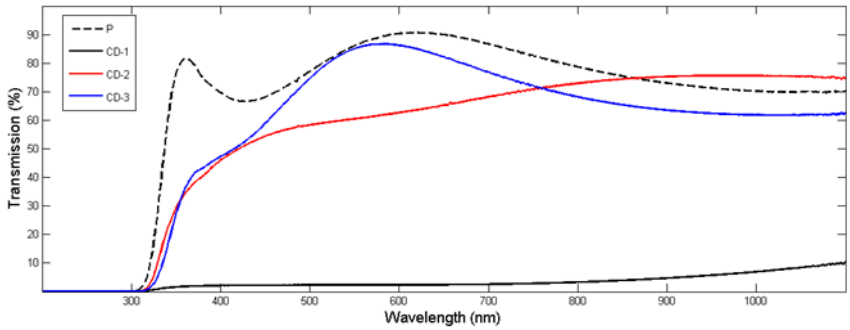

Figure 5.22 : Transparency of pure and N-Fe co-doped TiO_2 films.

From the absorption spectra of transparent, the wavelength of absorption edge increases by increasing the iron concentration. It might be due to the newly developed impurity states lay deep in the band gap of TiO_2 since they serve as recombination centers [79]. This result is in agreement with our previous study [77].

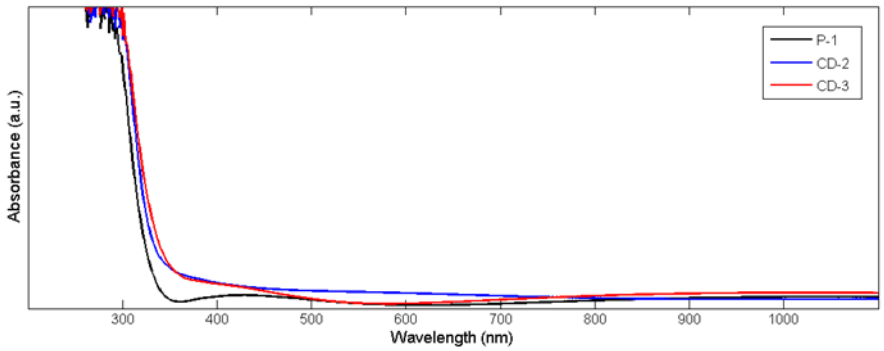

Figure 5.23 : UV-Vis optical absorption spectra of pure and N-Fe co-doped TiO_2 films

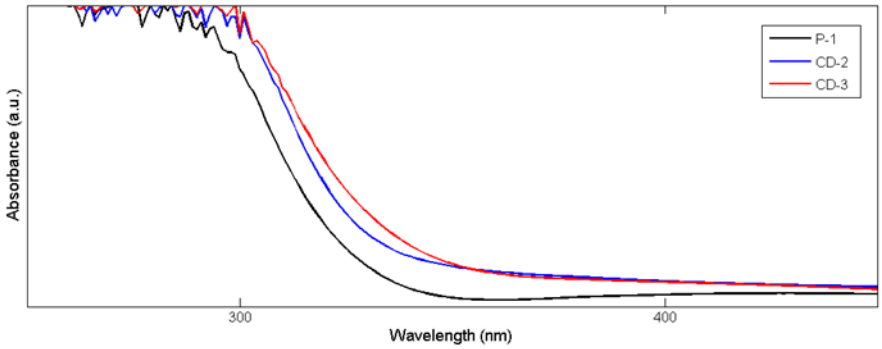

Figure 5.24 : UV-Vis optical absorption spectra of pure and N-Fe co-doped TiO_2 films

The reflectance spectra of pure and N-Fe co-doped TiO_2 films are shown in Fig. 5.25.

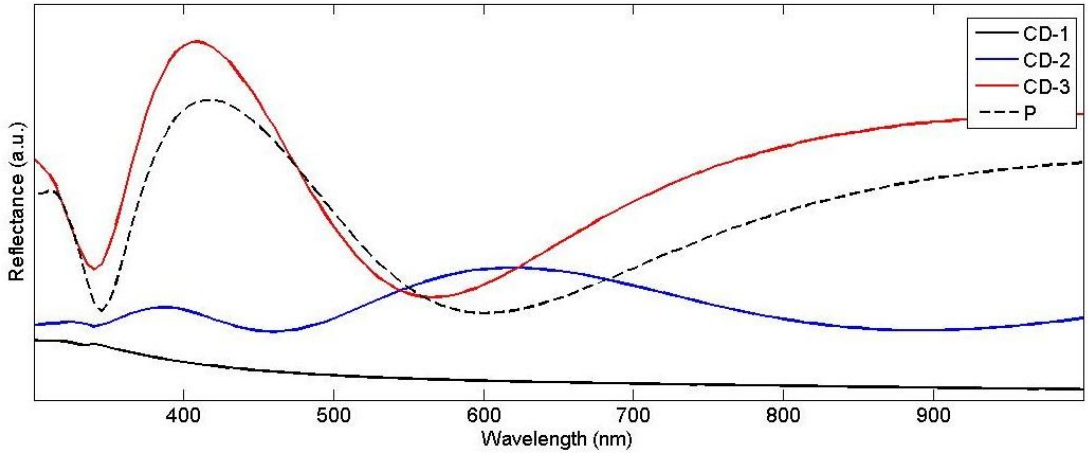

Figure 5.25 : UV-Vis optical reflectance spectra of pure and N-Fe co-doped TiO_2 films

The band-gap of prepared samples were calculated using Tauc plot method [80]. Tauc plots of prepared transparent samples are shown in Fig. 5.26. The absorption edge of the prepared pure TiO_2 thin film is about 330 nm which is lower than reported anatase pure TiO_2; therefore the band gap value obtained is about 3.55 eV, which is higher than the reported band gap value for crystalline anatase TiO_2. The high band gap value of the prepared film may be due to the thermal stress effects produced in the film [75]. This result is in agreement with the Welte et al [76]. The

CD-3 sample, which has more iron dopant concentration, has the lowest band-gap in the range of 3.2 eV.

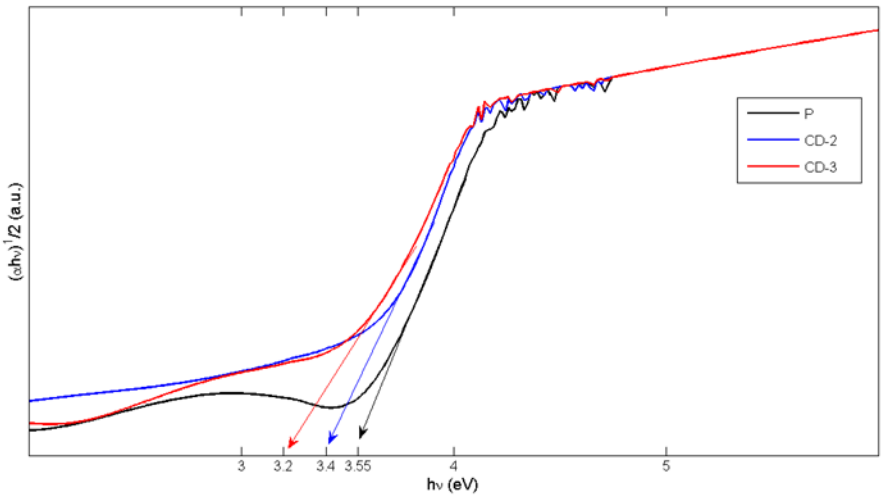

Figure 5.26 : Tauc plot of pure and N-Fe co-doped TiO_2 films.

5.3.5 Silver decorated TiO_2 thin films

5.3.5.1 Structural properties of silver decorated TiO_2 thin films

The XPS spectrum of AGC-4 film which is photodecomposed is reported in Fig 5.27 and the position of the Ti 2p3/2 peak (458 eV) is close to the reported value by reference and the oxidation level of titanium is +4 as expected.

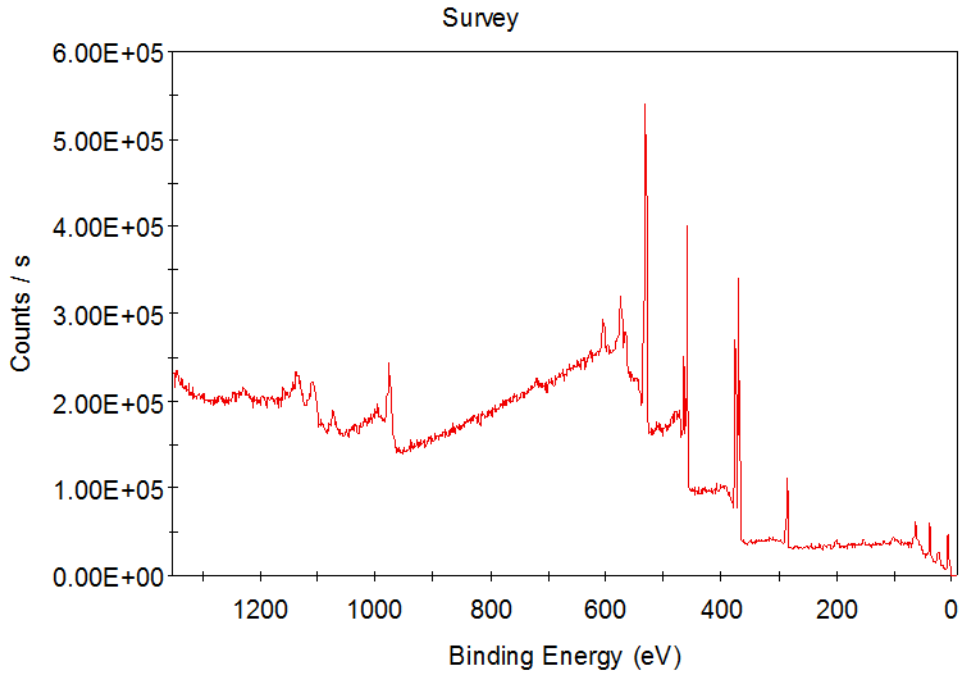

Figure 5.27 : XPS survey of AGC-4 sample.

The surface elemental analysis of AGC-4 sample result is shown in table 5.14 and reveal the presence of titanium and oxygen element as expected. Silver amount is around 7 atomic percent.

Table 5.14 : Elemental composition of AGC-4 thin film taken by XPS.

Element	Atomic %
Ti	23.86
O	60.08
C	24.2
Ag	7.2
N	1.26
TOTAL	100

The XPS spectrum of AGC-2 thin film which is thermal decomposed is showed in Fig. 5.28 and the position of the Ti 2p3/2 peak (458 eV) is close to the reported value by reference and the oxidation level of titanium is +4 as expected.

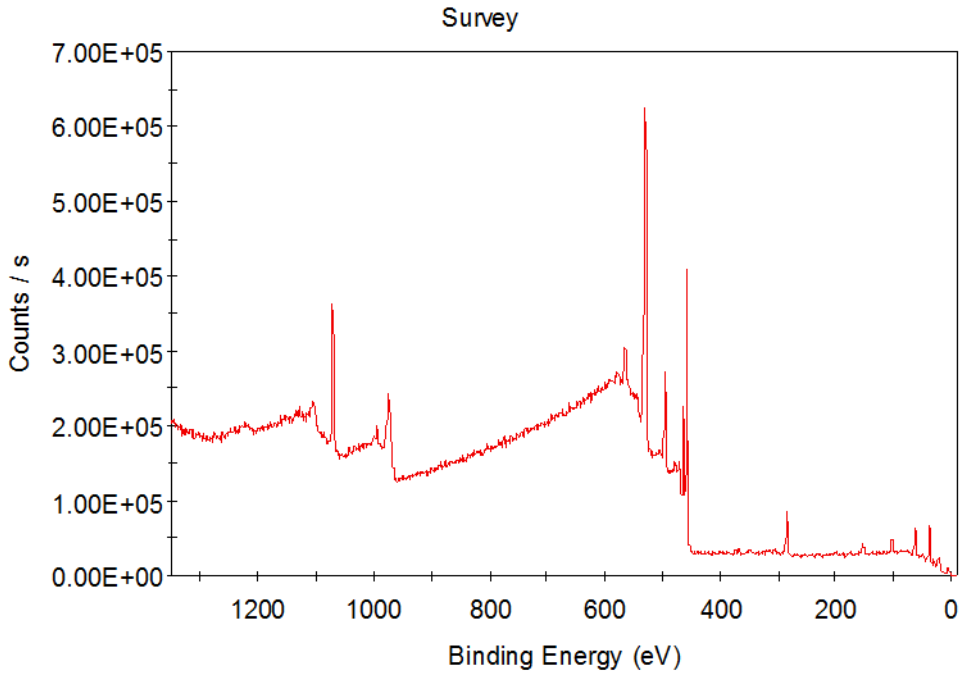

Figure 5.28 : XPS survey of AGC-2 sample.

The surface elemental analysis of AGC-2 sample is shown in table 5.15 and reveal the presence of titanium and oxygen element as expected. The amount of silver is too low in comparison with AGC-4 sample. It can be concluded that the silver reduction of photo-decomposition is much higher than thermal-decomposition.

Table 5.15 : Elemental composition of AGC-4 thin film taken by XPS.

Element	Atomic %
Ti	22.6
O	60.28
C	16.95
Ag	0.17
TOTAL	100

5.3.5.2 Optical properties of silver decorated TiO_2 thin films

The optical absorbance of Ag-decorated TiO_2 thin films are shown in Fig. 5.29 and state that the optical properties of TiO_2 is affected by thermal decomposition of silver negatively. The wavelength of the absorption is not changed by increasing the dipping speed. The wavelengths of optical absorption edge of the Ag-docorated TiO_2

thin films are shown in table 5.16 and show that the absorption edge of sample AGC-4 which was photodecomposed relies on visible light region.

Table 5.16 : Absorption edge of Ag decorated TiO_2.

Sample	Dipping speed of $Ag(NO)_3$ solution	Decomposition type	Wavelength of absorption edge (nm)
AGC-1	50	Thermal decomposition	340
AGC-2	150	Thermal decomposition	340
AGC-3	250	Thermal decomposition	340
AGC-4	150	Photo decomposition	380

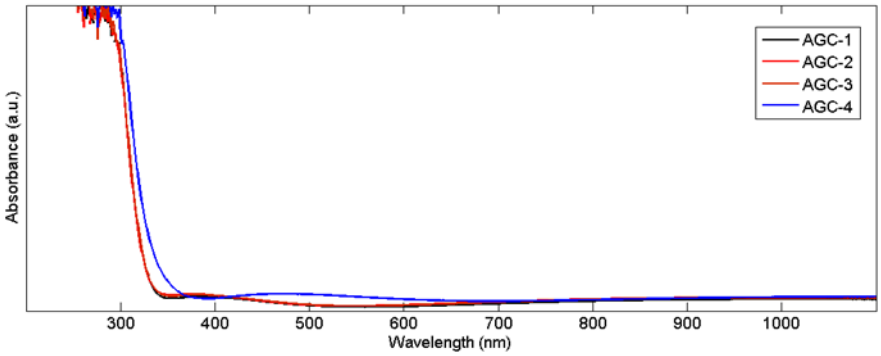

Figure 5.29 : UV-Vis optical absorption spectra of Ag decorated TiO_2 thin films

The Tauc plot of pure TiO_2 and silver decorated TiO_2 films are shown in Fig. 5.30 and reveal that thermal-decomposition has negative effect on optical properties and increases the band-gap of the films.

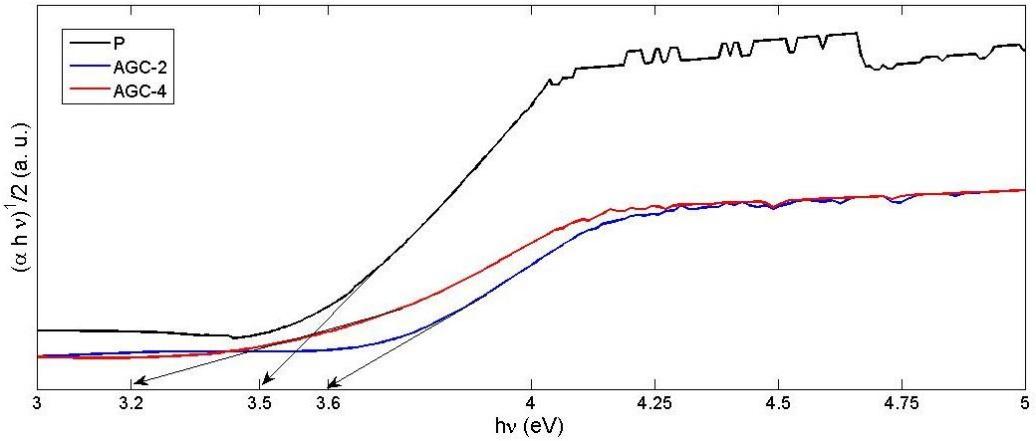

Figure 5.30 : Tauc plot of pure and silver decorated TiO_2 films.

5.3.6 Pure ZnO thin film

The absorption spectrum of pure ZnO is shown in Fig 5.31 and states that the absorption edge is around 340nm.

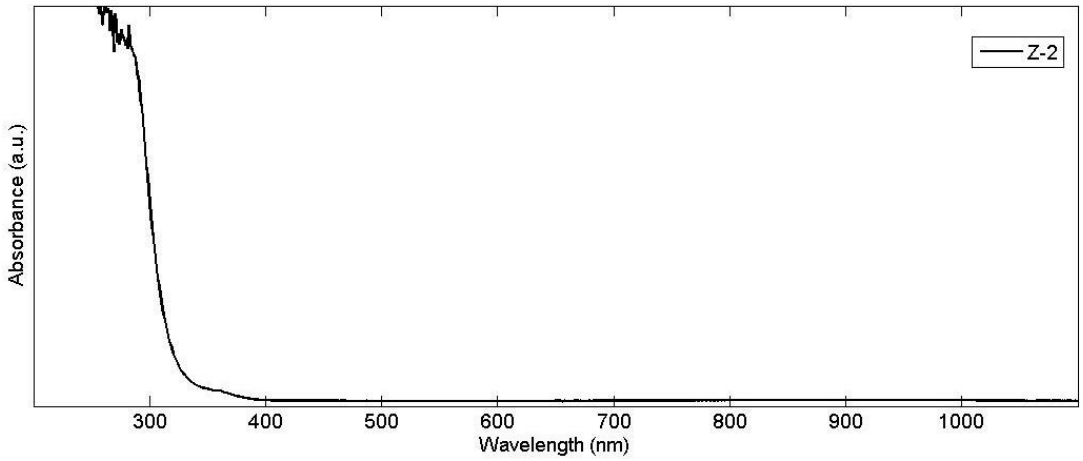

Figure 5.31 : UV-Vis absorption spectrum of pure ZnO thin film.

The reflectance spectrum of the pure ZnO sample is shown in Fig. 5.32.

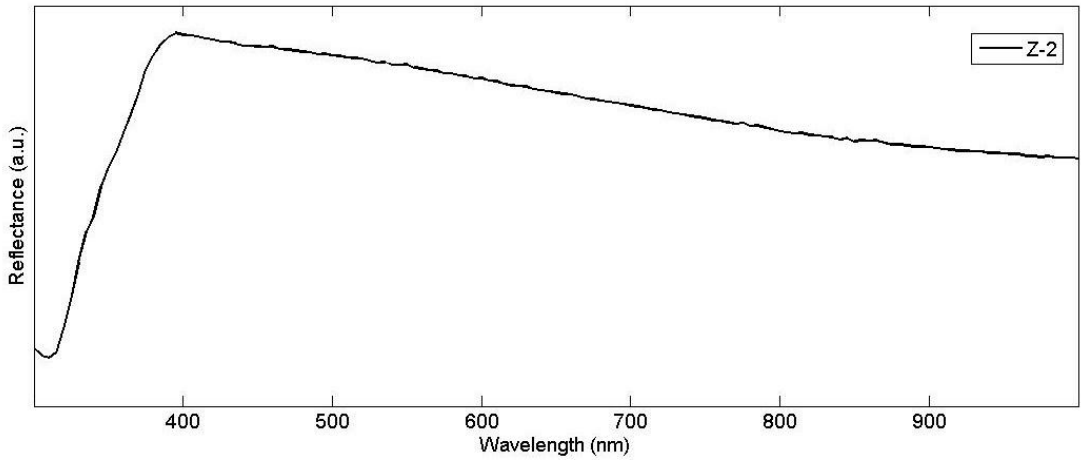

Figure 5.32 : UV-Vis reflectance spectrum of pure ZnO thin film.

The Tauc plot of pure ZnO is shown in Fig. 5.33 and it shows that the band gap of pure ZnO is around 3.6 eV which is higher than reported 3.4 eV. The high value of the band gap is related to the amorphous or low crystalline structure of the film [81].

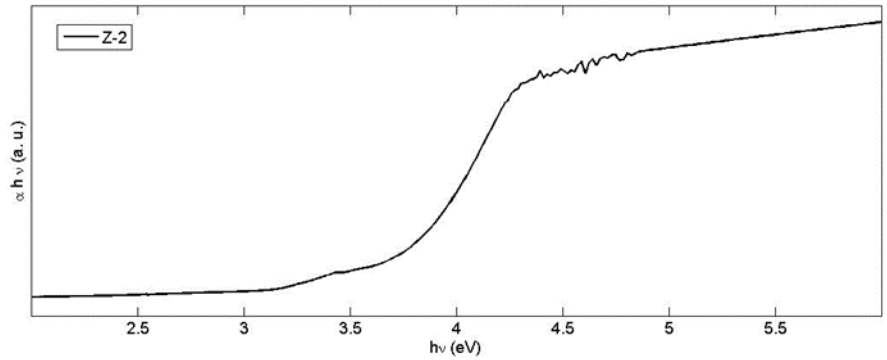

Figure 5.33 : Tauc plot of pure ZnO thin film.

5.3.7 TiO_2 @ ZnO composite thin films

5.3.7.1 Structural properties of TiO_2 @ ZnO composite thin films

The powder was obtained only in C-2 sample which is TiO_2 rich sample. The XRD pattern of C-2 sample is shown in Fig. and shows an amorphous structure.

5.3.7.2 Optical properties of TiO_2 @ ZnO composite thin films

The UV-Vis absorption spectra of transparent pure TiO_2 , pure ZnO and TiO_2 @ ZnO composite films are shown in Fig. 5.34.

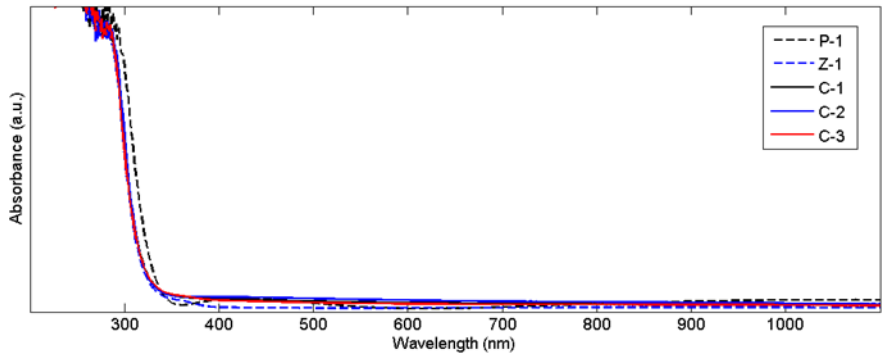

Figure 5.34 : UV-Vis optical absorption of TiO_2 @ ZnO composite thin films.

The absorption edge of the sample is related to the molar concentration. The absorption edge of C-2 sample (TiO_2 rich sample) is close to the pure TiO_2 absorption edge and the absorption edge of C-3 sample (ZnO rich sample) is close to the pure ZnO absorption edge as shown in Fig. 5.35.

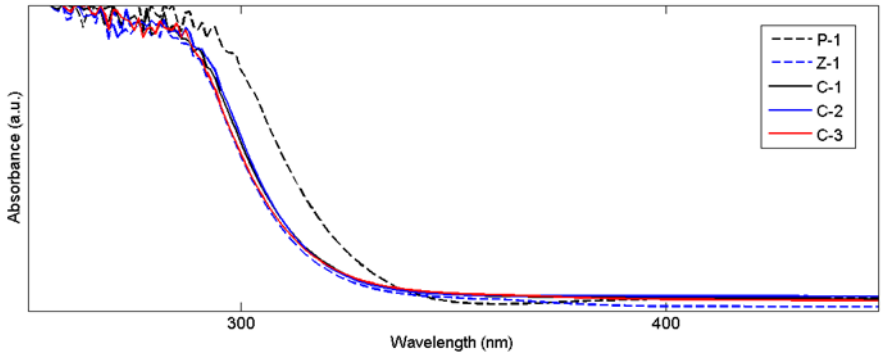

Figure 5.35 : Shifting of absorption edge in TiO_2 @ ZnO composite thin films.

The reflectance spectra of pure TiO_2, pure ZnO and TiO_2 @ ZnO composite thin films are shown in Fig 5.36. It shows that the by increasing the TiO_2 molar concentration the spectrum is closer to the pure TiO_2 spectrum.

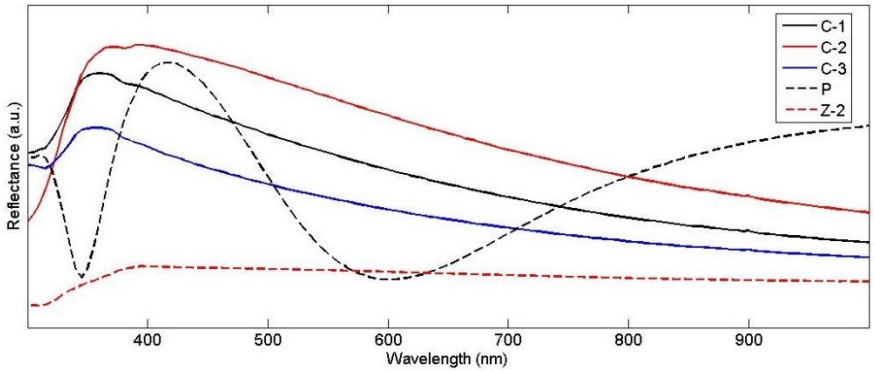

Figure 5.36 : UV-Vis reflectance spectra of pure TiO_2 , pure ZnO_2 and TiO_2 @ ZnO composite thin films

The Tauc plot of pure TiO_2 , pure ZnO and TiO_2 @ ZnO thin films are shown in Fig 5.37 and state that the band-gap of TiO_2 @ ZnO samples are higher than pure TiO_2 sample. The high band-gap of the composite samples are be attributed to the amorphous structure of those samples [81].

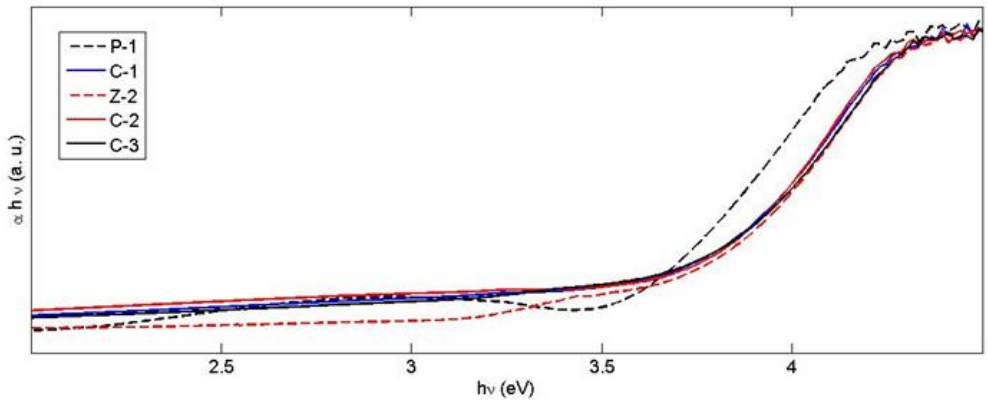

Figure 5.37 : Tauc plot of TiO_2 @ ZnO composite thin films.

The band-gap of composite films are closed to the band-gap of ZnO due to their amorphous structure as shown in Fig. 5.38.

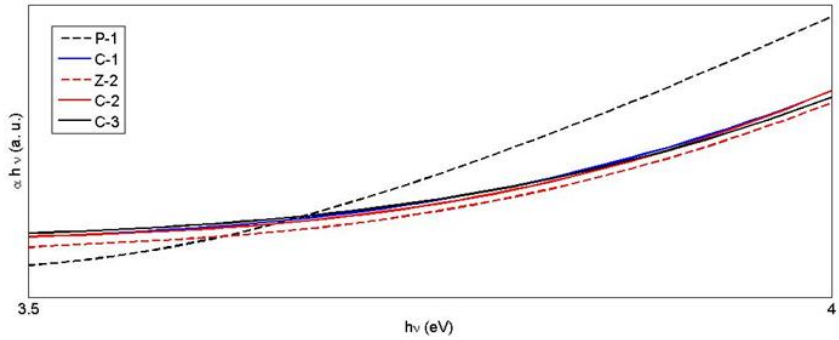

Figure 5.38 : Tauc plot of TiO_2 @ ZnO composite thin films.

6. CONCLUSION

The six different modified TiO_2 films were prepared by sol-gel dip-coating method and the effect of several parameters such dopant type, dopant concentration and other related parameters were investigated. The obtained results are summarized below:

- Nitrogen doped TiO_2 thin films: The optical absorbance of N-doped TiO_2 thin films state that the wavelength of the absorption edge does not increase by increasing the dopant concentration. The absorption edge of sample N-2 which is doped with 1.5 wt% nitrogen relies on visible light region. The lowest optical band-gap belongs to the sample N-2 which is doped with 1.5 wt% nitrogen.

- Iron doped TiO_2 thin films: The optical absorbance of Fe-doped TiO_2 thin films show that the wavelength of the absorption edge increases by increasing the dopant concentration. The absorption edges of sample F-2 and F-3 which doped with 1.5 wt% and 3 wt% iron rely on visible light region

- Silver doped TiO_2 thin films: The absorption edge of Ag-doped TiO_2 does not increase by increasing the dopant concentration. The absorption edge of silver doped samples do not rely on visible region.

- Nitrogen-iron co-doped TiO_2 films: The dopants ratio effects on resulting structure of samples. Sample with medium dopants concentration has amorphous structure and it may be attributed to the disordering of the TiO_2 lattice by the both iron and nitrogen atoms. It may attributed to the change of fractal dimension during film formation in dip-coating process. Pure TiO_2 and doped TiO_2 with dopants ratio of 33.7 have smaller particle size in the range of 25 – 35 nm. The CD-3 sample which has more iron dopant concentration has the lowest band-gap in the range of 3.2 eV. By changing the dopants ratio these features of N-Fe co-doped TiO_2 can be obtained:

  a) Transparent anatase b) Opaque amorphous c) Opaque anatase

- Silver decorated TiO_2 thin films: The optical properties of TiO_2 is affected by thermal decomposition of silver nitrate negatively. The wavelength of the absorption edge does not increase by increasing the dipping speed. The wavelengths of optical absorption edge of the Ag-docorated TiO_2 thin films show that the absorption edge of sample AGC-4 which was photodecomposed relies on visible light region.
- TiO_2 @ ZnO composite thin films: The absorption edge of the sample is related to the molar concentration. The absorption edge of C-2 sample (TiO_2 rich sample) is close to the pure TiO_2 absorption edge and the absorption edge of C-3 sample (ZnO rich sample) is close to the pure ZnO absorption edge.

REFERENCES

[1] **Clark, W., Broadhead, P.** (1970). Optical absorption and photochromism in iron-doped rutile. *Journal of Physics C: Solid State Physics*;3,5. p: 1047.

[2] **Willey, R. R.** (2002). Practical design and production of optical thin films: CRC Press.

[3] **Radecka, M., Zakrzewska, K., Czternastek, H., Stapiński, T., Debrus, S.** (1993). The influence of thermal annealing on the structural, electrical and optical properties of TiO 2-x thin films. *Applied surface science*;65. p: 227-34.

[4] **Lee, S., Oh, S.** (1997). In-situ Ellipsometric Investigation of TiO~ 2 Thin-Film Initial Growth. *JOURNAL-KOREAN PHYSICAL SOCIETY*;31. p: 352-6.

[5] **Orignac, X., Vasconcelos, H., Du, X., Almeida, R.** (1997). Influence of solvent concentration on the microstructure of SiO2-TiO2 sol-gel films. *Journal of Sol-Gel Science and Technology*;8,1-3. p: 243-8.

[6] **Hummel, R. E., Guenther, K. H.** (1995). Handbook of optical properties: thin films for optical coatings: CRC Press.

[7] **Fox, M. A., Dulay, M. T.** (1993). Heterogeneous photocatalysis. *Chemical reviews*;93,1. p: 341-57.

[8] **Kalyanasundaram, K., Grätzel, M.** (1994). Artificial photosynthesis: Efficient dye-sensitized photoelectrochemical cells for the direct conversion of sunlight to electricity. *Curr Science*;66. p: 706-15.

[9] **Mandelis, A.** (1993). Physics, chemistry and technology of solid state gas sensor devices: John Wiley & Sons.

[10] **Yamamoto, N., Tonomura, S., Tsubomura, H.** (1982). Temperature Dependence of the Sensitivities of Metal-TiO2 Junctions to Various Reducing Gases. *Journal of the Electrochemical Society*;129,2. p: 444-6.

[11] Standard CPDS X-ray diffraction spectra database.

[12] **Olsen, J. S., Gerward, L., Jiang, J.** (1999). On the rutile/α-PbO 2-type phase boundary of TiO 2. *Journal of Physics and Chemistry of Solids*;60,2. p: 229-33.

[13] **Dewhurst, J., Lowther, J.** (1996). High-pressure structural phases of titanium dioxide. *Physical Review B*;54,6. p: R3673.

[14] **Haines, J., Leger, J.** (1993). X-ray diffraction study of TiO 2 up to 49 GPa. *Physica B: Condensed Matter*;192,3. p: 233-7.

[15] **Mosaddeq-ur-Rahman, M., Miki, T., Krishna, K. M., Soga, T., Igarashi, K., Tanemura, S., et al.** (1996). Structural and optical characterization of Pb x Ti 1− x O 2 film prepared by sol-gel method. *Materials Science and Engineering: B*;41,1. p: 67-71.

[16] **Gotić, M., Ivanda, M., Sekulić, A., Musić, S., Popović, S., Turković, A., et al.** (1996). Microstructure of nanosized TiO 2 obtained by sol-gel synthesis. *Materials Letters*;28,1. p: 225-9.

[17] **Aarik, J., Aidla, A., Sammelselg, V., Siimon, H., Uustare, T.** (1996). Control of thin film structure by reactant pressure in atomic layer deposition of TiO 2. *Journal of crystal growth*;169,3. p: 496-502.

[18] **Bally, A.** (1999). Electronic properties of nano-crystalline titanium dioxide thin films: ÉCOLE POLYTECHNIQUE FÉDÉRALE DE LAUSANNE.

[19] **Wahlbeck, P. G., Gilles, P. W.** (1966). Reinvestigation of the phase diagram for the system titanium–oxygen. *Journal of the American Ceramic Society*;49,4. p: 180-3.
[20] **Goodenough, J., Hammett, A., Huber, G., Hulliger, F., Leiss, M., Ramasesha, S., et al.** (1984). Landolt-Börnstein III/17g. Springer Verlag, Berlin.
[21] **Bregani, F., Casale, C., Depero, L., Natali-Sora, I., Robba, D., Sangaletti, L., et al.** (1996). Temperature effects on the size of anatase crystallites in Mo□ TiO 2 and W□ TiO 2 powders. *Sensors and Actuators B: Chemical*;31,1. p: 25-8.
[22] **Serpone, N., Pelizzetti, E.** (1989). Photocatalysis: fundamentals and applications: Wiley New York.
[23] **Crittenden, J. C., Liu, J., Hand, D. W., Perram, D. L.** (1997). Photocatalytic oxidation of chlorinated hydrocarbons in water. *Water Research*;31,3. p: 429-38.
[24] **Hoffmann, M. R., Martin, S. T., Choi, W., Bahnemann, D. W.** (1995). Environmental applications of semiconductor photocatalysis. *Chemical reviews*;95,1. p: 69-96.
[25] **Angelidis, T., Koutlemani, M., Poulios, I.** (1998). Kinetic study of the photocatalytic recovery of Pt from aqueous solution by TiO 2, in a closed-loop reactor. *Applied Catalysis B: Environmental*;16,4. p: 347-57.
[26] **Fujishima, A., Zhang, X.** (2006). Titanium dioxide photocatalysis: present situation and future approaches. *Comptes Rendus Chimie*;9,5. p: 750-60.
[27] **Fujishima, A., Honda, K.** (1972). Electrochemical photolysis of water at a semiconductor electrode. *nature*238. p: 37-8.
[28] **Maeda, K., Domen, K.** (2010). Photocatalytic water splitting: recent progress and future challenges. *The Journal of Physical Chemistry Letters*;1,18. p: 2655-61.
[29] **Abe, R.** (2010). Recent progress on photocatalytic and photoelectrochemical water splitting under visible light irradiation. *Journal of Photochemistry and Photobiology C: Photochemistry Reviews*;11,4. p: 179-209.
[30] **Knox, V.** (2010). Review of Aurivillius photocatalysts. *AMERICAN CERAMIC SOCIETY BULLETIN*;89,5. p: 31-.
[31] **Wang, R., Hashimoto, K., Fujishima, A., Chikuni, M., Kojima, E., Kitamura, A., et al.** (1998). Photogeneration of highly amphiphilic TiO2 surfaces. *Advanced Materials*;10,2. p: 135-8.
[32] **Khataee, A., Kasiri, M. B.** (2010). Photocatalytic degradation of organic dyes in the presence of nanostructured titanium dioxide: Influence of the chemical structure of dyes. *Journal of Molecular Catalysis A: Chemical*;328,1. p: 8-26.
[33] **Brinker, C. J., Scherer, G. W.** (2013). Sol-gel science: the physics and chemistry of sol-gel processing: Academic press.
[34] **Corriu, R., Trong Anh, N.** (2009). Front Matter: Wiley Online Library.
[35] **Bahmani Jalali, H., Trabzon, L., Balaban, M., Kizil, H.** (2013). Effect of catalyst nature and its concentration on the sol-gel derived titanium dioxide particles. *Nano-TR Student Conference 2013*.
[36] **Carter, C. B., Norton, M. G.** Sols, gels, and organic chemistry. Ceramic Materials: Springer; 2013. p. 411-22.

[37] **Anpo, M.** (2000). Use of visible light. Second-generation titanium oxide photocatalysts prepared by the application of an advanced metal ion-implantation method. *Pure and applied chemistry*;72,9. p: 1787-92.
[38] **Fuerte, A., Hernandez-Alonso, M., Maira, A., Martinez-Arias, A., Fernandez-Garcia, M., Conesa, J., et al.** (2001). Visible light-activated nanosized doped-TiO 2 photocatalysts. *Chemical Communications*24. p: 2718-9.
[39] **Yamashita, H., Harada, M., Misaka, J., Takeuchi, M., Ichihashi, Y., Goto, F., et al.** (2001). Application of ion beam techniques for preparation of metal ion-implanted TiO2 thin film photocatalyst available under visible light irradiation: metal ion-implantation and ionized cluster beam method. *Journal of synchrotron radiation*;8,2. p: 569-71.
[40] **Ohno, T., Mitsui, T., Matsumura, M.** (2003). Photocatalytic Activity of S-doped TiO2 Photocatalyst under Visible Light. *Chemistry Letters*;32,4. p: 364-5.
[41] **Liu, Y., Chen, X., Li, J., Burda, C.** (2005). Photocatalytic degradation of azo dyes by nitrogen-doped TiO 2 nanocatalysts. *Chemosphere*;61,1. p: 11-8.
[42] **Yu, J. C., Zhang, L., Zheng, Z., Zhao, J.** (2003). Synthesis and characterization of phosphated mesoporous titanium dioxide with high photocatalytic activity. *Chemistry of Materials*;15,11. p: 2280-6.
[43] **Hirai, T., Suzuki, K., Komasawa, I.** (2001). Preparation and photocatalytic properties of composite CdS nanoparticles–titanium dioxide particles. *Journal of colloid and interface science*;244,2. p: 262-5.
[44] **Chatterjee, D., Mahata, A.** (2001). Demineralization of organic pollutants on the dye modified TiO 2 semiconductor particulate system using visible light. *Applied Catalysis B: Environmental*;33,2. p: 119-25.
[45] **Wang, J., Ma, T., Zhang, G., Zhang, Z., Zhang, X., Jiang, Y., et al.** (2007). Preparation of novel nanometer TiO 2 catalyst doped with upconversion luminescence agent and investigation on degradation of acid red B dye using visible light. *Catalysis Communications*;8,3. p: 607-11.
[46] **Zhou, W., Zheng, Y.-h., Wu, G.-h.** (2006). Novel luminescent RE/TiO 2 (RE= Eu, Gd) catalysts prepared by in-situation sol–gel approach construction of multi-functional precursors and their photo or photocatalytic oxidation properties. *Applied Surface Science*;253,3. p: 1387-92.
[47] **Asahi, R., Morikawa, T., Ohwaki, T., Aoki, K., Taga, Y.** (2001). Visible-light photocatalysis in nitrogen-doped titanium oxides. *science*;293,5528. p: 269-71.
[48] **Irie, H., Watanabe, Y., Hashimoto, K.** (2003). Nitrogen-concentration dependence on photocatalytic activity of TiO2-x N x powders. *The Journal of Physical Chemistry B*;107,23. p: 5483-6.
[49] **Ihara, T., Miyoshi, M., Iriyama, Y., Matsumoto, O., Sugihara, S.** (2003). Visible-light-active titanium oxide photocatalyst realized by an oxygen-deficient structure and by nitrogen doping. *Applied Catalysis B: Environmental*;42,4. p: 403-9.
[50] **Zhao, Z., Liu, Q.** (2008). Mechanism of higher photocatalytic activity of anatase TiO2 doped with nitrogen under visible-light irradiation from density functional theory calculation. *Journal of Physics D: Applied Physics*;41,2. p: 025105.

[51] **Sato, S.** (1986). Photocatalytic activity of NO x-doped TiO 2 in the visible light region. *Chemical Physics Letters*;123,1. p: 126-8.
[52] **Zhu, J., Zheng, W., He, B., Zhang, J., Anpo, M.** (2004). Characterization of Fe–TiO 2 photocatalysts synthesized by hydrothermal method and their photocatalytic reactivity for photodegradation of XRG dye diluted in water. *Journal of Molecular Catalysis A: Chemical*;216,1. p: 35-43.
[53] **Lee, M. S., Hong, S.-S., Mohseni, M.** (2005). Synthesis of photocatalytic nanosized TiO 2–Ag particles with sol–gel method using reduction agent. *Journal of Molecular Catalysis A: Chemical*;242,1. p: 135-40.
[54] **Li, Q., Li, Y. W., Wu, P., Xie, R., Shang, J. K.** (2008). Palladium Oxide Nanoparticles on Nitrogen-Doped Titanium Oxide: Accelerated Photocatalytic Disinfection and Post-Illumination Catalytic "Memory". *Advanced Materials*;20,19. p: 3717-23.
[55] **Chen, X., Wang, X., Hou, Y., Huang, J., Wu, L., Fu, X.** (2008). The effect of postnitridation annealing on the surface property and photocatalytic performance of N-doped TiO 2 under visible light irradiation. *Journal of Catalysis*;255,1. p: 59-67.
[56] **Cong, Y., Zhang, J., Chen, F., Anpo, M., He, D.** (2007). Preparation, photocatalytic activity, and mechanism of nano-TiO2 co-doped with nitrogen and iron (III). *The Journal of Physical Chemistry C*;111,28. p: 10618-23.
[57] **Li, X., Chen, Z., Shi, Y., Liu, Y.** (2011). Preparation of N, Fe co-doped TiO 2 with visible light response. *Powder Technology*;207,1. p: 165-9.
[58] **Hu, S., Li, F., Fan, Z., Chang, C.-C.** (2011). Enhanced photocatalytic activity and stability of nano-scaled TiO 2 co-doped with N and Fe. *Applied Surface Science*;258,1. p: 182-8.
[59] **Fan, J. W., Liu, J. Y., Hong, J., Zhang, J.** (2009). The synthesis of nanostructure TiO2 co-doped with N and Fe and their application for micro-polluted source water treatment. *Environmental technology*;30,13. p: 1447-52.
[60] **Huang, K., Chen, L., Xiong, J., Liao, M.** (2012). Preparation and characterization of visible-light-activated Fe-N Co-doped TiO 2 and its photocatalytic inactivation effect on leukemia tumors. *International Journal of Photoenergy*;2012.
[61] **Kim, T.-H., Rodríguez-González, V., Gyawali, G., Cho, S.-H., Sekino, T., Lee, S.-W.** (2013). Synthesis of solar light responsive Fe, N co-doped TiO 2 photocatalyst by sonochemical method. *Catalysis Today*;212. p: 75-80.
[62] **Lee, Y. K., Jung, C. H., Park, J., Seo, H., Somorjai, G. A., Park, J. Y.** (2011). Surface plasmon-driven hot electron flow probed with metal-semiconductor nanodiodes. *Nano letters*;11,10. p: 4251-5.
[63] **Ingram, D. B., Linic, S.** (2011). Water splitting on composite plasmonic-metal/semiconductor photoelectrodes: evidence for selective plasmon-induced formation of charge carriers near the semiconductor surface. *Journal of the American Chemical Society*;133,14. p: 5202-5.
[64] **Mayer, K. M., Hafner, J. H.** (2011). Localized surface plasmon resonance sensors. *Chemical reviews*;111,6. p: 3828-57.
[65] **Lu, Y., Yu, H., Chen, S., Quan, X., Zhao, H.** (2012). Integrating plasmonic nanoparticles with TiO2 photonic crystal for enhancement of visible-

light-driven photocatalysis. *Environmental science & technology*;46,3. p: 1724-30.
[66] **Tian, Y., Tatsuma, T.** (2005). Mechanisms and applications of plasmon-induced charge separation at TiO2 films loaded with gold nanoparticles. *Journal of the American Chemical Society*;127,20. p: 7632-7.
[67] **Rycenga, M., Cobley, C. M., Zeng, J., Li, W., Moran, C. H., Zhang, Q., et al.** (2011). Controlling the synthesis and assembly of silver nanostructures for plasmonic applications. *Chemical reviews*;111,6. p: 3669-712.
[68] **Xie, K., Sun, L., Wang, C., Lai, Y., Wang, M., Chen, H., et al.** (2010). Photoelectrocatalytic properties of Ag nanoparticles loaded TiO 2 nanotube arrays prepared by pulse current deposition. *Electrochimica Acta*;55,24. p: 7211-8.
[69] **Wang, Q., Yang, X., Liu, D., Zhao, J.** (2012). Fabrication, characterization and photocatalytic properties of Ag nanoparticles modified TiO 2 NTs. *Journal of Alloys and Compounds*;527. p: 106-11.
[70] **Linsebigler, A. L., Lu, G., Yates Jr, J. T.** (1995). Photocatalysis on TiO2 surfaces: principles, mechanisms, and selected results. *Chemical reviews*;95,3. p: 735-58.
[71] **Hurum, D. C., Agrios, A. G., Gray, K. A., Rajh, T., Thurnauer, M. C.** (2003). Explaining the enhanced photocatalytic activity of Degussa P25 mixed-phase TiO2 using EPR. *The Journal of Physical Chemistry B*;107,19. p: 4545-9.
[72] **Hurum, D. C., Gray, K. A., Rajh, T., Thurnauer, M. C.** (2005). Recombination pathways in the Degussa P25 formulation of TiO2: surface versus lattice mechanisms. *The Journal of Physical Chemistry B*;109,2. p: 977-80.
[73] **Leytner, S., Hupp, J. T.** (2000). Evaluation of the energetics of electron trap states at the nanocrystalline titanium dioxide/aqueous solution interface via time-resolved photoacoustic spectroscopy. *Chemical Physics Letters*;330,3. p: 231-6.
[74] **Sadeghvaziri, N., Rezvani, M., Bahmani Jalali, H., Bolandi, B.** (2013). Self-cleaning property of cerium doped titanium dioxide coated soda-lime glass prepared by sol-gel process: Effect of dopant concentration. *The 9th Congress of Iranian Ceramic Society*;Sharif University of Technology, Tehran, Iran
[75] **Yu, J., Xiong, J., Cheng, B., Liu, S.** (2005). Fabrication and characterization of Ag–TiO 2 multiphase nanocomposite thin films with enhanced photocatalytic activity. *Applied Catalysis B: Environmental*;60,3. p: 211-21.
[76] **Welte, A., Waldauf, C., Brabec, C., Wellmann, P. J.** (2008). Application of optical absorbance for the investigation of electronic and structural properties of sol–gel processed TiO 2 films. *Thin Solid Films*;516,20. p: 7256-9.
[77] **Bahmani Jalali, H., Trabzon, L., Kizil, H.** (2014). Characterization and Comparison of Visible Light Active Fe-Doped and N-doped TiO 2 Films Prepared by Sol-Gel Process. *Australian Journal of Basic & Applied Sciences*;8,23.
[78] **Brinker, C., Frye, G., Hurd, A., Ashley, C.** (1991). Fundamentals of sol-gel dip coating. *Thin Solid Films*;201,1. p: 97-108.

[79] **Asahi, R., Morikawa, T.** (2007). Nitrogen complex species and its chemical nature in TiO 2 for visible-light sensitized photocatalysis. *Chemical Physics*;339,1. p: 57-63.
[80] **Tauc, J.** (1968). Optical properties and electronic structure of amorphous Ge and Si. *Materials Research Bulletin*;3,1. p: 37-46.
[81] **Lindroos, S., Leskelä, M.** (2000). Growth of zinc peroxide (ZnO 2) and zinc oxide (ZnO) thin films by the successive ionic layer adsorption and reaction–SILAR–technique. *International Journal of Inorganic Materials*;2,2. p: 197-201.

CURRICULUM VITAE

Name Surname: Houman BAHMANI JALALI

Place and Date of Birth: Tabriz, Iran - 19/07/1989

E-Mail: hbahmanijalali@gmail.com

EDUCATION:

B.Sc. : Materials Engineering – University of Tabriz, Iran

PROFESSIONAL EXPERIENCE AND REWARDS:

- Research Assistant at ITUnano Nanotechnology Research Center, Istanbul Technical University (2013-now)
- Research Assistant at ITU-MEMS Research Laboratory, Istanbul Technical University (2013-now)
- Research Assistant at Nano Fluid Laboratory, Faculty of Mechanical Engineering, University of Tabriz (2012-2013)

- Synthesis of ultra-homogeneous spherical silica nanoparticles at Nano Fluid Laboratory of University of Tabriz first time in Iran. This honour was awarded by Ministry of Science of Iran (2013)

PUBLICATIONS, PRESENTATIONS AND PATENTS ON THE THESIS:

- H. Bahmani Jalali, L. Trabzon "Influence of dopants ratio on structure and optical properties N-Fe co-doped TiO_2 films prepared via sol-gel dip-coating" (under review)
- H. Bahmani Jalali et al. " A comparative study on optical properties of silver doped and silver decorated TiO_2 thin films prepared by sol-gel dip-coating method" , IMAGINENANO 2015 conference, Bilbao, Spain (2015 March)
- H. Bahmani Jalali et al. "Characterization and Comparison of Visible Light Active Fe-Doped and N-doped TiO_2 Films Prepared by Sol-Gel Process", Australian Journal of Basic and Applied Sciences, 8(23) Special 2014, Pages: 259-263
- H. Bahmani Jalali et al. "Preparation, structural and optical characterization of visible light active iron doped TiO_2 films", ACE-X 2014 conference, Paris, France (2014 July)
- H. Bahmani Jalali et al. "Effect of catalyst nature and its concentration on the sol-gel derived TiO_2 particles", NANO-TR student conference, Istanbul Technical University, Istanbul, Turkey (2013 October)

OTHER PUBLICATIONS, PRESENTATIONS AND PATENTS:

- E. Esmaeilzadeh et al. "Synthesis of spherical silica particles using sol-gel method by hydrolysis and condensation of Tetraethyl orthosilicate in aprotic solvents", Advanced Materials World Conference (2013 September)
- N. Sadeghvaziri et al. "Self-cleaning property of cerium doped titanium dioxide coated soda-lime glass prepared by sol-gel process: Effect of dopant concentration", 9th Iranian Ceramics Congress,Tehran, Iran (2013 May)